JVI Journals.ASM.org

Effects of Toll-Like Receptor Stimulation on Eosinophilic Infiltration in Lungs of BALB/c Mice Immunized with UV-Inactivated Severe Acute Respiratory Syndrome-Related Coronavirus Vaccine

Naoko Iwata-Yoshikawa,[a] Akihiko Uda,[b] Tadaki Suzuki,[a] Yasuko Tsunetsugu-Yokota,[c]* Yuko Sato,[a] Shigeru Morikawa,[b] Masato Tashiro,[d] Tetsutaro Sata,[a] Hideki Hasegawa,[a] Noriyo Nagata[a]

Department of Pathology,[a] Department of Veterinary Science,[b] Department of Immunology,[c] and Influenza Virus Research Center,[d] National Institute of Infectious Diseases, Tokyo, Japan

ABSTRACT

Severe acute respiratory syndrome-related coronavirus (SARS-CoV) is an emerging pathogen that causes severe respiratory illness. Whole UV-inactivated SARS-CoV (UV-V), bearing multiple epitopes and proteins, is a candidate vaccine against this virus. However, whole inactivated SARS vaccine that includes nucleocapsid protein is reported to induce eosinophilic infiltration in mouse lungs after challenge with live SARS-CoV. In this study, an ability of Toll-like receptor (TLR) agonists to reduce the side effects of UV-V vaccination in a 6-month-old adult BALB/c mouse model was investigated, using the mouse-passaged Frankfurt 1 isolate of SARS-CoV. Immunization of adult mice with UV-V, with or without alum, resulted in partial protection from lethal doses of SARS-CoV challenge, but extensive eosinophil infiltration in the lungs was observed. In contrast, TLR agonists added to UV-V vaccine, including lipopolysaccharide, poly(U), and poly(I·C) (UV-V+TLR), strikingly reduced excess eosinophilic infiltration in the lungs and induced lower levels of interleukin-4 and -13 and eotaxin in the lungs than UV-V-immunization alone. Additionally, microarray analysis showed that genes associated with chemotaxis, eosinophil migration, eosinophilia, and cell movement and the polarization of Th2 cells were upregulated in UV-V-immunized but not in UV-V+TLR-immunized mice. In particular, CD11b$^+$ cells in the lungs of UV-V-immunized mice showed the upregulation of genes associated with the induction of eosinophils after challenge. These findings suggest that vaccine-induced eosinophil immunopathology in the lungs upon SARS-CoV infection could be avoided by the TLR agonist adjuvants.

IMPORTANCE

Inactivated whole severe acute respiratory syndrome-related coronavirus (SARS-CoV) vaccines induce neutralizing antibodies in mouse models; however, they also cause increased eosinophilic immunopathology in the lungs upon SARS-CoV challenge. In this study, the ability of adjuvant Toll-like receptor (TLR) agonists to reduce the side effects of UV-inactivated SARS-CoV vaccination in a BALB/c mouse model was tested, using the mouse-passaged Frankfurt 1 isolate of SARS-CoV. We found that TLR stimulation reduced the high level of eosinophilic infiltration that occurred in the lungs of mice immunized with UV-inactivated SARS-CoV. Microarray analysis revealed that genes associated with chemotaxis, eosinophil migration, eosinophilia, and cell movement and the polarization of Th2 cells were upregulated in UV-inactivated SARS-CoV-immunized mice. This study may be helpful for elucidating the pathogenesis underlying eosinophilic infiltration resulting from immunization with inactivated vaccine.

Severe acute respiratory syndrome-related coronavirus (SARS-CoV), a cause of severe respiratory illness, emerged in southern China in late 2002 and quickly spread to several countries throughout Asia, Europe, and North America by early 2003 (1–4). Although SARS has not reemerged since 2003, vaccination is the most likely mode of preventing future SARS-CoV outbreaks, especially in individuals at high risk, such as health care workers. To date, no vaccine is licensed for SARS-CoV. A SARS-CoV vaccine based on whole inactivated virions is easily prepared and is expected to induce a broader spectrum of antibodies than recombinant virus-based vaccines expressing particular sets of SARS-CoV proteins. Although inactivated whole SARS-CoV vaccines induce neutralizing antibodies in mouse models (5–10), they also cause increased eosinophilic immunopathology in the lungs upon SARS-CoV challenge (11–14). These reactions are thought to be caused by the incorporation of SARS-CoV nucleocapsid protein (N) in vaccine formulations, which induces N-specific immune responses and enhances eosinophilic immune pathology (11, 12, 15).

Enhanced eosinophilic immune pathology was also observed in the 1960s, when formalin-inactivated respiratory syncytial virus (FI-RSV) vaccine combined with alum adjuvant was injected intramuscularly into children to immunize them against RSV. In these trials, 80% of immunized children were hospitalized and died of enhanced respiratory disease upon subsequent RSV infec-

Received 8 April 2014 **Accepted** 13 May 2014
Published ahead of print 21 May 2014
Editor: S. Perlman
Address correspondence to Noriyo Nagata, nnagata@niid.go.jp.
* Present address: Yasuko Tsunetsugu-Yokota, Tokyo University of Technology, Tokyo, Japan.
Supplemental material for this article may be found at http://dx.doi.org/10.1128/JVI.00983-14.
Copyright © 2014, American Society for Microbiology. All Rights Reserved.
doi:10.1128/JVI.00983-14

tion. Histologic examination of their lungs showed bronchoconstriction and severe pneumonia with peribronchiolar eosinophils (16, 17). These findings suggest that FI-RSV vaccination induced nonneutralizing, nonprotective antibodies, with natural infection of RSV causing a hypersensitivity response to viral antigens, characterized by bronchoconstriction and severe pneumonia. The pathology of the enhanced respiratory disease upon subsequent RSV infection is thought to be due to skewing of the immune response toward Th2, with eosinophils having a key role in the progression of enhanced respiratory disease. The generation of nonprotective antibodies by the FI-RSV vaccine may have been due to poor Toll-like receptor (TLR) stimulation (18).

Thus, TLR stimulation with an inactivated whole virion vaccine is thought to be crucial to induce protective antibodies and to reduce eosinophilic responses. In this study, we evaluated the efficacy and safety of UV-inactivated whole SARS-CoV (UV-V) in a model using BALB/c mice and mouse-passaged SARS-CoV. We investigated the ability of adjuvant TLR agonists to reduce the side effects of UV-V vaccination, such as enhanced eosinophilic immune pathology.

MATERIALS AND METHODS

Viruses and cells. Vero E6 cells, purchased from the American Type Culture Collection (Manassas, VA), were cultured in Eagle's minimal essential medium (MEM) containing 5% fetal bovine serum (FBS), 50 IU/ml penicillin G, and 50 μg/ml streptomycin. Stocks of the mouse-passaged Frankfurt 1 isolate of SARS-CoV, F-musX-VeroE6 (F-musX), were propagated and titrated on Vero E6 cells and cryopreserved at −80°C as previously described (19). Viral infectivity titers are expressed as 50% of the tissue culture infectious dose ($TCID_{50}$)/ml on Vero E6 cells, as calculated according to the Behrens-Kärber method. Work with infectious SARS-CoV was performed under biosafety level 3 conditions.

Preparation of UV-V. UV-V was prepared as previously described (6). Briefly, the HKU39849 isolate of SARS-CoV was amplified in Vero E6 cells, exposed to UV light (4.75 J/cm^2), and purified by sucrose density gradient centrifugation. Inactivation of the virus infectivity of UV-V was confirmed upon inoculation into Vero E6 cells.

Animal experiments. BALB/c female mice, purchased from Japan SLC Inc. (Shizuoka, Japan), were housed in an environmentally controlled specific-pathogen-free animal facility. Animals were infected with SARS-CoV in biosafety level 3 animal facilities, according to the Animal Care and Use Committee of the National Institute of Infectious Diseases, Tokyo, Japan.

For immunization, 14-week-old BALB/c mice were subcutaneously injected in the back with 10 μg UV-V alone (UV-V), 10 μg UV-V plus 2 mg alum (Pierce, Rockford, IL) (UV-V+Alum), or 10 μg UV-V plus TLR agonists (UV-V+TLR) and reimmunized 6 to 7 weeks later. The TLR agonists consisted of 1 μg lipopolysaccharide (LPS) (Sigma-Aldrich, St. Louis, MO), 2.5 μg poly(I·C) (Invitrogen, San Diego, CA), and 0.1 μg poly(U) (Invitrogen) per immunization. Control mice were injected with phosphate-buffered saline (PBS) with or without alum.

At 8 to 10 days after the 2nd immunization, mice were anesthetized by intraperitoneal injection of a mixture of 1.0 mg ketamine and 0.02 mg xylazine in 0.1 ml/10 g body weight. The animals were subsequently inoculated in the left nostril with $10^{6.5}$ $TCID_{50}$ of F-musX in 30 μl, 1,000-fold higher than the 50% lethal dose for adult BALB/c mice ($n = 5$ to 7 per group) (19).

A second vaccination experiment was performed to evaluate the long-term efficacy of TLR, with the vaccinated mice rested for 4 weeks before F-musX challenge. Ten-week-old BALB/c mice were vaccinated with 10 μg UV-V or 10 μg UV-V+TLR and boosted 6 weeks later. Four weeks afterwards, the animals were inoculated in the left nostril with $10^{6.5}$ $TCID_{50}$ in 30 μl of F-musX.

To mimic immunization with an attenuated vaccine, 25-week-old mice were administered $10^{6.3}$ $TCID_{50}$ of the HKU39849 isolate in 20 μl intranasally, since HKU39849 was shown to be avirulent in adult mice. Control mice were injected with MEM intranasally. Fourteen days later, these mice were challenged intranasally with $10^{6.5}$ $TCID_{50}$ in 30 μl of F-musX.

Body weights were measured daily for 10 days, and the mice were sacrificed 3 or 10 days after challenge to analyze virus replication, hematology, cytokine expression, and pathology ($n = 3$ to 4 per group).

Virus titration. To titrate virus infectivity in lung homogenates, 10% (wt/vol) tissue homogenates of each lung were prepared in MEM containing 2% FBS, 50 IU/ml penicillin G, 50 μg/ml streptomycin, and 2.5 μg/ml amphotericin B. Lung wash fluid was also collected for analysis of infectious virus titers.

Cytokine and chemokine profiling. Inflammatory profiling of 10% (wt/vol) lung homogenates was performed using the Milliplex Map assay (Millipore, MA), as described by the manufacturer. These assays can determine the concentrations of 18 cytokines and chemokines, including eotaxin, granulocyte-macrophage colony-stimulating factor (GM-CSF), gamma interferon (IFN-γ), interleukin 1β (IL-1β), IL-2, IL-4, IL-5, IL-6, IL-7, IL-10, IL-12 (p70), IL-13, gamma interferon-induced protein 10 (IP-10), neutrophil-related chemokine KC (KC), monocyte chemoattractant protein 1 (MCP-1), macrophage inflammatory protein 1α (MIP-1α), regulated and normal T cell expressed and secreted (RANTES), and tumor necrosis factor alpha (TNF-α). Type I IFNs in 10% (wt/vol) lung homogenates obtained 3 and 10 days after inoculation were analyzed using mouse alpha and beta IFN (IFN-α and -β) enzyme-linked immunosorbent assay (ELISA) kits (PBL Interferon Source, Piscataway, NJ), according to the protocol described by the manufacturer.

SARS-CoV neutralizing assay. Blood was obtained from the tail vein of each mouse and allowed to clot. Sera were collected by centrifugation and inactivated by incubation at 56°C for 30 min. One hundred $TCID_{50}$ aliquots of F-musX of SARS-CoV were incubated for 1 h in the presence or absence of mice sera serially 2-fold diluted and then added to confluent Vero E6 cell cultures in 96-well microtiter plates as described previously (20). The presence of a viral cytopathic effect was determined on day 3, and the titers of neutralizing antibody were determined as the reciprocal of the highest dilution at which cytopathic effect was not observed. The lowest and highest serum dilutions tested were 1:2 and 1:512, respectively.

Quantitative real-time reverse transcription (RT)-PCR. To assay type I IFN mRNA expression and viral genome copies during early phases of SARS-CoV infection, the left lobe of a lung from mice injected with UV-V ($n = 6$), UV-V+TLR ($n = 6$), or PBS ($n = 3$) was obtained 1 day after challenge and placed in RNAlater solution (Ambion). RNA was extracted from the lung samples using RNeasy minikits (Qiagen, Hilden, Germany), according to the manufacturer's instructions.

Real-time one-step quantitative RT-PCR assays were used to detect IFN-α4, IFN-β, and SARS-CoV mRNA using QuantiTect Probe RT-PCR kits (Qiagen, Valencia, CA) and an ABI Prism 7900HT Fast real-time PCR system (Applied Biosystems, Foster City, CA). TaqMan probes and primers are listed in Table 1. Reaction mixtures were incubated at 50°C for 30 min, followed by 95°C for 15 min and thermal cycling, which consisted of 40 cycles of denaturation at 94°C for 15 s, and annealing and extension at 60°C for 60 s. The expression of each gene was normalized relative to that of β-actin mRNA, with the expression of IFN-α4 and IFN-β mRNAs calculated as the $\log_{10}$ fold change relative to results with PBS-injected and challenged mice.

Histopathology and immunohistochemistry. Animals were anesthetized and perfused with 2 ml of 10% phosphate-buffered formalin ($n = 3$ to 4). Animals were necropsied within 12 h of death, whereas moribund animals were euthanized by excess isoflurane. All animals were subsequently examined histopathologically, with 10% phosphate-buffered formalin injected into the trachea until the lungs inflated. Fixed lung tissues were routinely embedded in paraffin, sectioned, and stained with hematoxylin and eosin. Eosinophils were identified with a C.E.M. kit using

TABLE 1 Primers and probes for quantitative real-time RT-PCR

Target (reference)	Sequence
IFN-α4	
Forward	CAACTCTACTAGACTCATTCTGCAAT
Reverse	AGAGGAGGTTCCTGCATCACA
Probe	ACCTCCATCAGCAGCTCAATGACCTCAAA
IFN-β	
Forward	GCTCCTGGAGCAGCTGAATG
Reverse	TCCGTCATCTCCATAGGGATCT
Probe	TCAACCTCACCTACAGGGCGGACTTC
SARS-CoV N gene (56)	
Forward	AGGAACTGGCCCAGAAGCTT
Reverse	AACCCATACGATGCCTTCTTTG
Probe	ACTTCCCTACGGCGCTA
β-Actin	
Forward	ACGGCCAGGTCATCACTATTG
Reverse	CAAGAAGGAAGGCTGGAAAAGA
Probe	CAACGAGCGGTTCCGATGCCC

Astra Blue/Vital New Red staining (DBS, Pleasanton, CA). For Astra Blue/Vital New Red-stained slides, five 240-μm^2 sections in the extrabronchioles were assessed, and the eosinophils, neutrophils, lymphocytes, and macrophages counted were averaged per lung of each mouse. Immunohistochemical detection of SARS-CoV antigens was performed on paraffin-embedded sections, as previously described (19).

Isolation of CD11b-positive ($CD11b^+$) lung cells. Whole lungs were collected from mice 1 day after challenge with F-musX, and their $CD11b^+$ cells were isolated by a modification of previous protocols (21). Briefly, mice were euthanized under excess anesthesia, and the lungs were perfused via the left ventricle with 20 ml of PBS containing 10 U/ml of heparin (Novo Nordisk Pharma Ltd., Novo Alle, Denmark) to remove red blood cells (RBCs). The lungs were removed aseptically, cut into 1-mm pieces, and incubated in HEPES buffer containing collagenase D (2 mg/ml; Roche Applied Science, Mannheim, Germany) and bovine pancreatic DNase I (40 U/ml; Sigma-Aldrich) for 30 to 45 min at 37°C. Single-cell suspensions were prepared by gently pushing the tissue through a 70-μm nylon screen, followed by washing and centrifugation at 2,000 rpm. To isolate $CD11b^+$ cells, the single-cell suspensions were washed with PBS containing 0.5% FBS (PBS-FBS), counted, and incubated at the appropriate ratio with MACS CD11b microbeads (Miltenyi Biotec, Auburn, CA) for 15 min at 4°C. After washing again with 10 ml of PBS-FBS, the cells were diluted in 3 ml of PBS-FBS. Finally, the $CD11b^+$ cells were separated by passing the antibody-coated cell suspension over an MS-positive selection column on a SuperMACS magnetic cell separator (Milteni Biotec). $CD11b^+$ cells were collected by removing the column from the magnetic field and then flushing it with PBS-FBS. Purity was checked by flow cytometry. To confirm the morphology of the obtained cells, around 1×10^5 cells in 100 μl of PBS-FBS were centrifuged at 1,000 rpm for 10 min onto glass slides using a Shandon cytocentrifuge (Thermo Fisher Scientific Inc., Waltham, MA). These cells were stained with Giemsa stain and analyzed by microscopy.

Flow cytometry analysis. The lung $CD11b^+$ cells were washed with PBS-FBS. After blocking Fc receptors by incubating 1 μg of anti-mouse CD16/CD32 monoclonal antibody (MAb) (BD Pharmingen, San Jose, CA) per 10^6 cells for 20 min on ice, the cells were stained for 30 min on ice with allophycocyanin (APC)-conjugated anti-mouse CD11b (BioLegend Inc., San Diego, CA). The cells were washed twice in PBS-FBS and fixed with 2% paraformaldehyde. Flow cytometry was performed on a FACSCanto II instrument (Becton, Dickinson, San Diego, CA), with the data analyzed using the FlowJo 8.7.1 software program (Treestar, Ashland, OR).

Microarray analysis. Microarray analysis was performed using left lung lobe tissue samples and $CD11b^+$ cells in the lung, as described previously (22). Briefly, total RNA was extracted using an RNeasy minikit (Qiagen, Hilden, Germany), according to the manufacturer's instructions. RNA concentrations were measured with an ND-1000 spectrophotometer (Nanodrop Technologies, Wilmington, DE). The quality of the RNA samples was assessed spectroscopically, and the quality of the intact RNA was assessed using an Agilent 2100 bioanalyzer (Agilent Technologies, Inc., Palo Alto, CA). RNA samples with the highest RNA integrity number, of more than 7, as determined by the bioanalyzer, were used for microarray analysis. Two hundred micrograms (lung tissue) or 25 μg ($CD11b^+$ cells) of total RNAs was used for amplification and labeled using a low-RNA-input linear amplification kit (Agilent).

Individual cRNA samples were fragmented by incubation with fragmentation buffer and blocking agent at 60°C for 30 min (gene expression hybridization kit [Agilent]). These RNA samples were hybridized at 65°C for 17 h at 10 rounds per min to a SurePrint G3 Mouse GE 8 by 60,000 microarray (Agilent). Controls consisted of RNA samples from mice injected with PBS, applied in duplicate to the slides; single samples were applied for all other RNA samples. The microarray slides were washed with wash solutions 1 and 2 (Agilent) and acetonitrile (Wako, Osaka, Japan). The slides were scanned with a DNA microarray scanner (Agilent), the images were analyzed using the Feature Extraction software program (Agilent), and the data files were automatically exported. Data mining was performed using the GeneSpring GX 12.1 software program (Agilent). Briefly, the text file exported by Feature Extraction software was imported into GeneSpring. The raw data were normalized per chip to the 75th percentile expression level and per gene to the median expression intensity of all samples. The samples of lung tissue were classified into four groups based on the treatment regimen: six mice each were immunized with UV-V, UV-V+TLR, and HKU39849, and three mice each were injected with PBS, yielding a total of six microarrays because the PBS samples were run in duplicate. $CD11b^+$ cell samples were classified into four groups based on the treatment regimen: six mice each were infected with F-musX and immunized with UV-V or UV-V+TLR, and six mice each were mock infected and immunized with UV-V or UV-V+TLR. Since the differences in individual gene expression within each group were small, all data are presented as the mean per group. Significant differences in gene expression between the UV-V and UV-V+TLR groups was assessed using one-way analysis of variance (ANOVA), followed by Tukey's honestly significant difference *post hoc* test and the Benjamini-Hochberg correction test, with P values of ≤ 0.05 considered statistically significant, and further filtered by $\geq$2-fold expression. Genes that met these criteria were characterized using Ingenuity Pathway Analysis (IPA) (Ingenuity Systems, Redwood City, CA) function annotations. All microarray slide hybridizations were performed using mouse oligonucleotide arrays (G4852A; Agilent).

Statistical analysis. Intergroup comparisons were performed by one-way ANOVA followed by Turkey's *post hoc* test using the GraphPad Prism 5 software program (GraphPad Software Inc., CA). P values less than 0.05 were considered statistically significant.

Microarray data accession numbers. The microarray results obtained in this work have been deposited in the Gene Expression Omnibus (GEO) (http://www.ncbi.nlm.nih.gov/projects/geo/) and assigned accession numbers GSE44274 (lung tissue) and GSE50855 ($CD11b^+$ cells isolated from lung).

RESULTS

Immunization with UV-V induces eosinophilic infiltrations in the lungs of adult mice after SARS-CoV challenge. To confirm an induction of eosinophilic immunopathology by immunization with UV-V in the adult mouse model (19), 11 mice per group were immunized with the vaccine and challenged 10 days after boosting with the live virus. All of the control mice, injected with PBS and alum (PBS+Alum), died of acute respiratory illness within 5 days

after infection with the live virus (Fig. 1A). In contrast, UV-V+Alum-immunized mice showed mild illness, such as hunching, ruffled fur, and body weight loss, within 3 days of infection and then recovered by day 5 (Fig. 1A). UV-V-immunized mice showed various levels of body weight loss and respiratory illness upon virus challenge. One mouse immunized with UV-V and one immunized with UV-V+Alum died on day 5. Virus titers in the lungs on day 3 did not differ significantly among UV-V-immunized, UV-V+Alum-immunized, and PBS+Alum-injected mice ($n = 3$ each) (Fig. 1B). In contrast, titers of virus in lung wash fluid on day 3 were significantly lower in UV-V+Alum-immunized mice than in PBS+Alum-injected mice. On the day before challenge with live virus, the serum titers of neutralizing antibodies were significantly higher in UV-V+Alum- than in UV-V-immunized mice ($n = 11$ each) (Fig. 1C) but did not differ significantly after challenge. The PBS+Alum-injected mice did not show seroconversion against SARS-CoV after challenge. Microscopic analysis of the lung sections of mice at 3 days after infection showed a high level of eosinophil infiltration around the bronchi in UV-V- and UV-V+Alum-immunized mice (Fig. 1D), whereas lymphocytes, macrophages, and a few neutrophils had infiltrated into the lungs of PBS+Alum-injected mice (Fig. 1D). Eosinophil infiltration was more severe on day 10 than on day 3 in UV-V- and UV-V+Alum-immunized mice. Histopathologically, both UV-V- and UV-V+Alum-immunized mice showed infiltration of inflammatory cells, including eosinophils, surrounding the bronchi and blood vessels on day 3 ($n = 3$ each) (Fig. 1E), consistent with previous results (13). We also investigated the lung pathology of the mice that died by day 5. Surprisingly, the lungs of both the UV-V- and UV-V+Alum-immunized mice showed high eosinophilic infiltration into areas surrounding the bronchi and blood vessels and severe inflammatory infiltrations in the alveoli (Fig. 2). Immunohistochemical analysis showed that a few SARS-CoV antigen-positive cells were present in the bronchiolar epithelial cells and alveolar cells of the dead UV-V-immunized mouse but were not present in cells of the dead UV-V+Alum-immunized mouse (Fig. 2). Although the virus neutralization titers in the sera on the day prior to virus challenge were 1:4 and 1:128 in the UV-V- and UV-V+Alum-immunized mice, respectively, these mice were unable to survive following SARS-CoV infection. In contrast, PBS+Alum-injected mice showed severe pulmonary edema, congestion, and hemorrhage, with many viral antigen-positive cells in the alveoli 5 days after challenge. We assumed that the severe respiratory illness in the dead UV-V- and UV-V+Alum-immunized mice was caused by an exacerbation of pulmonary inflammatory reactions due to UV-V acting as an inactivated RSV vaccine (18). The excess pulmonary eosinophilic infiltration possibly resulted from host immune responses rather than from a direct cytopathic effect caused by SARS-CoV replication.

Considering the excess eosinophilic immunopathology following SARS-CoV infection in mice immunized with inactivated virus, we examined whether the natural course of immune response elicited after nonlethal SARS-CoV infection resulted in excess eosinophil infiltration in the lungs of the reinfected mice. Mice were infected with the HKU39849 isolate, which induces nonlethal infection of both young and adult BALB/c mice, and challenged with F-musX. None of the HKU39849-inoculated mice showed clinical illness, as assessed by the absence of ruffled fur, dyspnea, and weight loss, and all survived after F-musX challenge (Fig. 3A). Titers of virus in the lungs of control mice were high on day 3 (10^8 $TCID_{50}$/g), although titers in the lungs and lung wash fluids of HKU39849-inoculated mice on days 3 and 10 after challenge were below the limit of detection (Fig. 3B). Virus neutralization titers in the sera on the day prior to virus challenge were higher than 1:16 (Fig. 3C). Histopathologically, the lungs of HKU39849-inoculated mice showed mild perivascular and peribronchiolar mononuclear cell infiltration on days 3 and 10 after the challenge (Fig. 3D and E). Most of these infiltrating cells were lymphocytes, with no eosinophils, and there were no cells positive for viral antigens in the lungs. In contrast, MEM-treated control mice showed severe respiratory illness and weight loss after F-musX infection and succumbed to infection within 5 days (Fig. 3A). The lung pathology of these control mice was similar to that of PBS+Alum-injected mice following challenge with SARS-CoV (data not shown). Thus, inoculation with HKU39849, mimicking immunization with attenuated live vaccine, provided a high level of protective immunity against SARS-CoV infection and elicited mild lymphocytic but not eosinophil infiltration in the lung after reinfection with F-musX.

Immunization with UV-V plus TLR agonists inhibits skewing to a Th2 response and high eosinophilic infiltration into the lungs of adult mice after challenge infection. We hypothesized that the excess pulmonary eosinophilic infiltration observed in mice immunized with UV-V was due to poor Toll-like receptor (TLR) stimulation as shown in FI-RSV vaccination (18). TLR agonists were used to induce host immune responses, especially innate immune responses, to virus infection (23, 24). Recognition by TLRs induces innate immune responses and eventually leads to activation of antigen-specific immunity (23). In addition, inactivated RSV vaccine-induced pulmonary disease was resolved by the addition of TLR agonists in an RSV mouse model (18). Therefore, we investigated the effect of TLR agonists as an adjuvant during immunization with UV-V. Within 3 days of challenge infection, UV-V+TLR-immunized mice developed a clinical illness, characterized by weight loss, hunching, and ruffled fur, but recovered by day 4 (Fig. 4A). By day 10, the body weight of all mice had recovered to that before immunization, and no mice had died (Fig. 4B). The survival rates, weight loss, and clinical illness of UV-V- and UV-V+TLR-immunized mice did not differ significantly. Viral titers in lung wash fluid but not in the lungs were significantly lower in UV-V+TLR-immunized mice than in PBS-injected mice on day 3 postinfection (p.i.) (Fig. 4C). Both UV-V- and UV-V+TLR-immunized mice showed seroconversion against SARS-CoV after the booster injection, with the titers of neutralizing antibodies on day 10 tending to be higher in UV-V+TLR-immunized than in UV-V-immunized mice (Fig. 4D). Interestingly, slight eosinophilic infiltration was observed in the lungs of UV-V+TLR-immunized mice on day 3 but not on day 10 (Fig. 4E). On day 10, lymphocytes were the primary infiltrating cells around vessels in the lungs of these mice. The numbers of eosinophils in the lungs were significantly lower in UV-V+TLR-immunized than in UV-V-immunized mice (Fig. 4F). Cytokine and chemokine responses were assessed in lung homogenates of UV-V- and UV-V+TLR-immunized mice on days 3 and 10. The levels of the Th2-related inflammatory cytokines IL-4 and IL-13 and the eosinophil-related chemokine eotaxin (CCL11) were lower in UV-V+TLR- than in UV-V-immunized mice on days 3 and 10 (Fig. 5). In contrast, the levels of IP-10 (CXCL10) and KC (CXCL1) tended to be higher in UV-V+TLR- than in UV-V-immunized mice on day 3. There were no significant

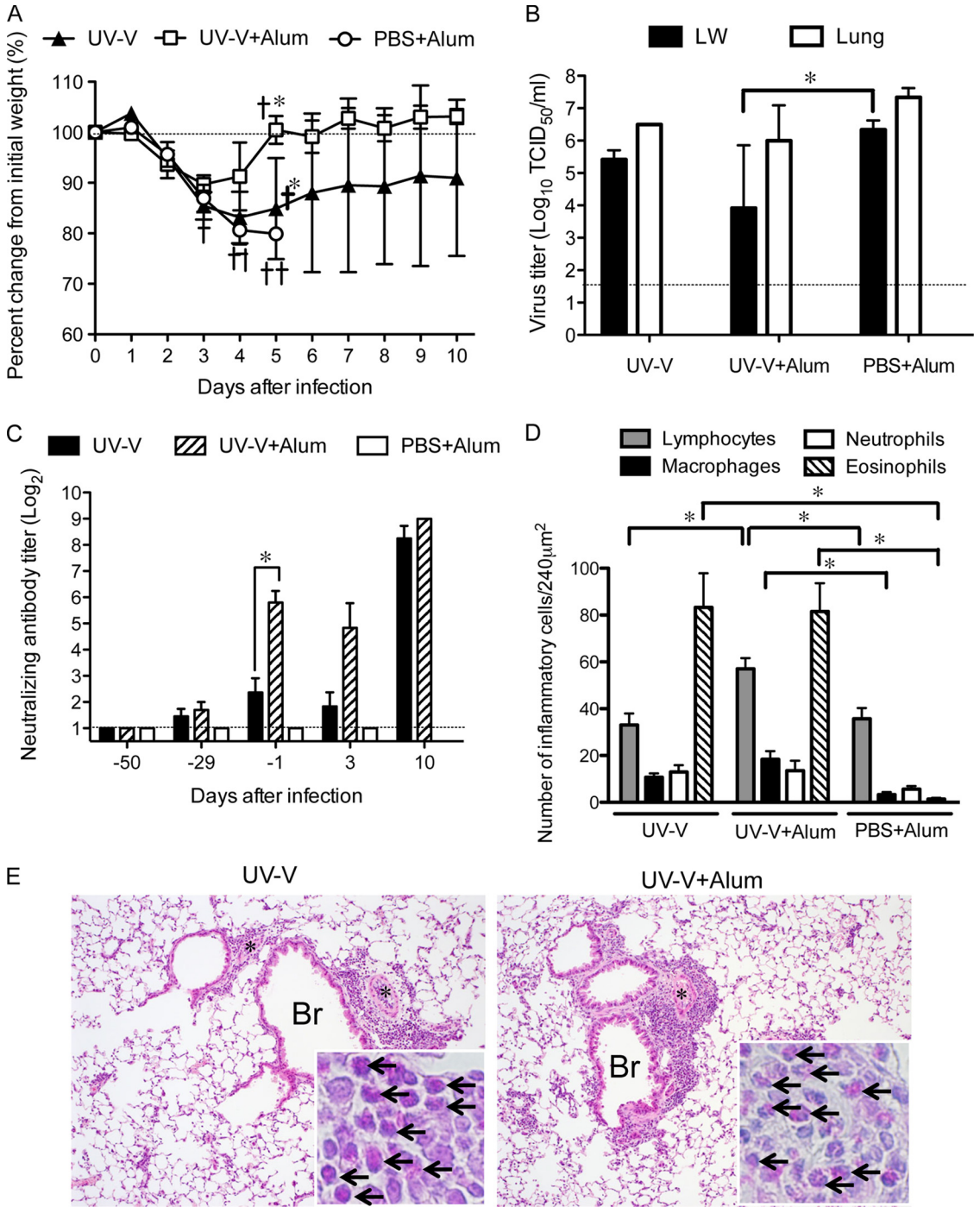

FIG 1 Immunization with UV-V induces eosinophilic immune pathology in adult mice after SARS-CoV challenge. Adult female BALB/c mice were vaccinated with UV-V, UV-V with alum (UV-V+Alum), or vehicle (PBS with Alum, PBS+Alum) and subsequently challenged with 1,000 $TCID_{50}$ of F-musX. (A) Body weight changes following the challenge inoculation ($n = 5$). Dead mice are marked with crosses. Error bars indicate standard deviations. Significant differences ($P < 0.05$, one-way ANOVA) between groups are marked with an asterisk. (B) Virus titers in the lungs and lung wash fluids on day 3 postchallenge ($n = 3$). The dashed line indicates the limit of detection ($10^{1.5}$ $TCID_{50}$/ml). Error bars indicate standard deviation. Significant differences ($P < 0.05$, one-way ANOVA) between groups are marked with an asterisk. LW, lung wash fluid. (C) Neutralizing serum antibody titers against SARS-CoV on days 50, 29, and 1 before challenge ($n = 11$) and on days 3 and 10 after challenge ($n = 5$ to 6). Serum samples were 2-fold serially diluted beginning at 1:2. Error bars indicate standard deviations. Significant differences ($P < 0.05$, one-way ANOVA) between groups are marked with an asterisk. (D) Numbers of lymphocytes, macrophages, neutrophils, and eosinophils in lung sections ($n = 3$) on day 3 after challenge. Five 240-μm^2 regions in the extrabronchioles of lung per mouse were examined at magnification ×40. Asterisks indicate $P < 0.05$ by the Bonferroni test. Error bars indicate standard deviations. (E) Representative images of lung sections from UV-V- and UV+Alum-immunized mice on day 10 postchallenge. Hematoxylin-and-eosin (magnification, ×10) and C.E.M. kit (inset; magnification, ×100) staining were used. Br, bronchi; *, blood vessel.

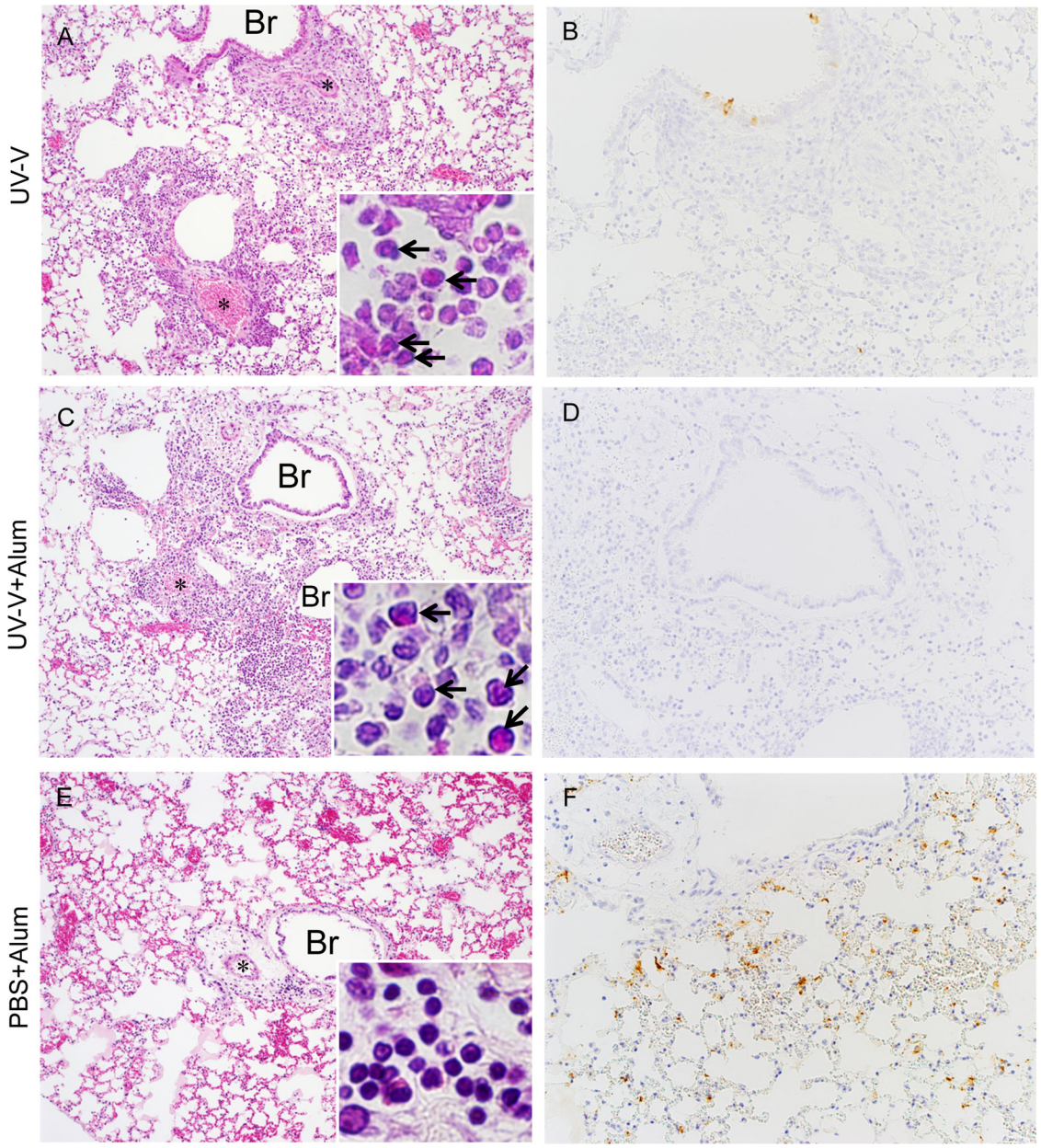

FIG 2 Histopathological findings in the lungs of dead mice after SARS-CoV challenge. Lungs were obtained for pathological examination (A, C, and E) and immunohistochemical analysis of SARS-CoV virus antigens (B, D, and F) from mice that died 5 days after challenge. Br, bronchi; *, blood vessel. Severe inflammatory infiltrates containing eosinophils were observed in the lungs of the UV-V-immunized mouse (A, inset). A few virus antigens were present in the bronchi (B). The UV-V+Alum-immunized mouse also showed eosinophilic inflammatory reactions, but no viral antigen-positive cells were present in the lungs (C, inset, and D). Congestion, hemorrhage, and pulmonary edema with mononuclear cell infiltration were observed in the mock-vaccinated mouse (PBS+Alum) (E, inset). Cells positive for viral antigen were seen throughout the lung (F). Hematoxylin-and-eosin (magnification, ×10) and C.M.E kit (inset; magnification, ×100) staining, a reliable and specific stain for eosinophils (A, C, and E), or immunohistochemical staining with an anti-SARS-CoV antibody (magnification, ×20) (B, D, and F) were used.

differences among UV-V-immunized, UV-V+TLR-immunized, and PBS+Alum-injected mice in the levels of other proinflammatory cytokines and chemokines, including GM-CSF, IFN-γ, IL-12p70, IL-1b, IL-2, IL-5, IL-6, IL-7, MCP-1, MIP-1α, RANTES, and TNF-α. These results indicate that TLR agonists are potent adjuvants that inhibit the skewing of immune responses toward Th2 responses and block the enhanced eosinophilic infiltration into the lungs that occurs after SARS-CoV infection.

Immunization with UV-V plus TLR agonists induces IFN-β gene expression in the lungs after challenge. Stimulation of TLRs-3,-4, and -7 by TLR agonists induces type I IFNs, with the induction of these type I IFNs being the most immediate antiviral host response to many viral infections (25). To confirm the effect due to poly(I·C) injection before challenge in UV-V+TLR-immunized mice, we employed quantitative real-time RT-PCR to assess mRNA expression levels in UV-V- and UV-V+TLR-immunized mice ($n = 6$) 1 day after challenge. The amount of IFN-α4

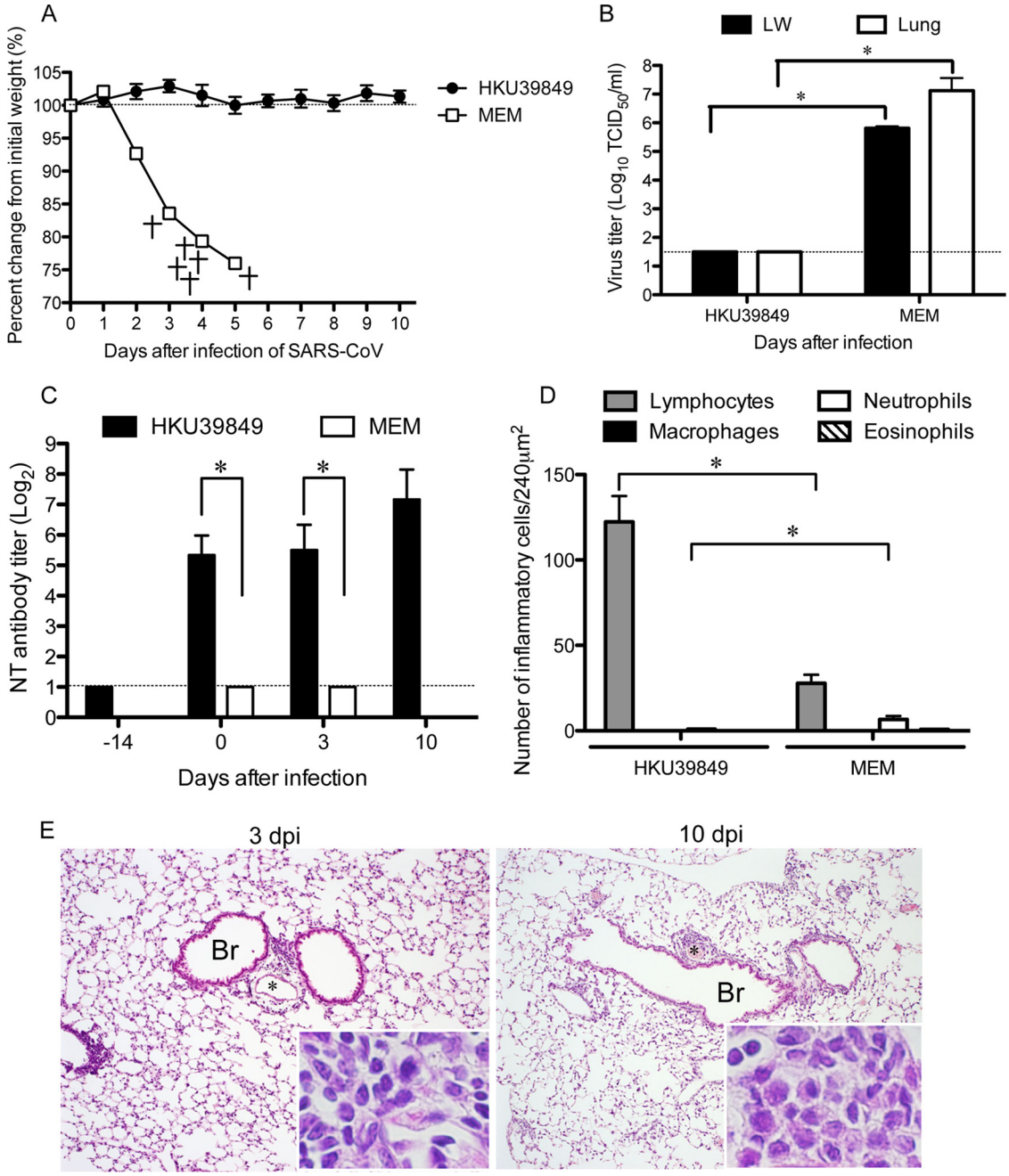

FIG 3 Reinfection with SARS-CoV in aged mice. Aged mice were infected with the HKU39849 isolate or mock vaccinated (no vaccination) and subsequently infected with 1,000 $TCID_{50}$ of F-musX. (A) Mice were weighed daily after challenge. All mock-vaccinated mice died by day 5, but all reinfected mice survived. Dead mice are marked with crosses. Error bars indicate standard deviations. (B) Virus titers in the lungs and lung wash fluids 3 days after challenge ($n = 3$). The dashed line indicates the limit of detection ($10^{1.5}$ $TCID_{50}$/ml). Error bars indicate standard deviations. Significant between-group differences ($P < 0.05$ by one-way ANOVA) are marked with an asterisk. LW, lung wash fluid. (C) Neutralizing serum antibody titers against SARS-CoV on days 0, 3, and 10 after challenge ($n = 6$ to 12). Serum samples were 2-fold serially diluted beginning at 1:2. Error bars indicate standard deviations. Significant between-group differences ($P < 0.05$ by one-way ANOVA) are marked with an asterisk. (D) Numbers of lymphocytes, macrophages, neutrophils, and eosinophils in lung sections ($n = 3$) 3 days after challenge. Five 240-μm^2 regions in the extrabronchioles of each mouse lung were examined at magnification ×40. Asterisks indicate $P < 0.05$ by the Bonferroni test. Error bars indicate standard deviations. (E) Representative images of the lungs of SARS-CoV-reinfected mice. Br, bronchi; *, blood vessel. Lung samples taken 3 and 10 days after infection were sectioned and stained with hematoxylin and eosin (magnification, ×10) and the C.E.M. kit (inset; magnification, ×100).

mRNA did not differ significantly in the lung tissues of UV-V- and UV-V+TLR-immunized mice. Although IFN-β gene expression in the lungs was significantly higher in UV-V+TLR- than in UV-V-immunized mice on day 1 (Fig. 6A), the viral copy number in the lungs of these mice did not differ significantly (Fig. 6B). In addition, ELISAs showed that IFN-α and -β in the sera and lungs of UV-V- and UV-V+TLR- and PBS-infected mice were below the limits of detection 3 and 10 days after challenge.

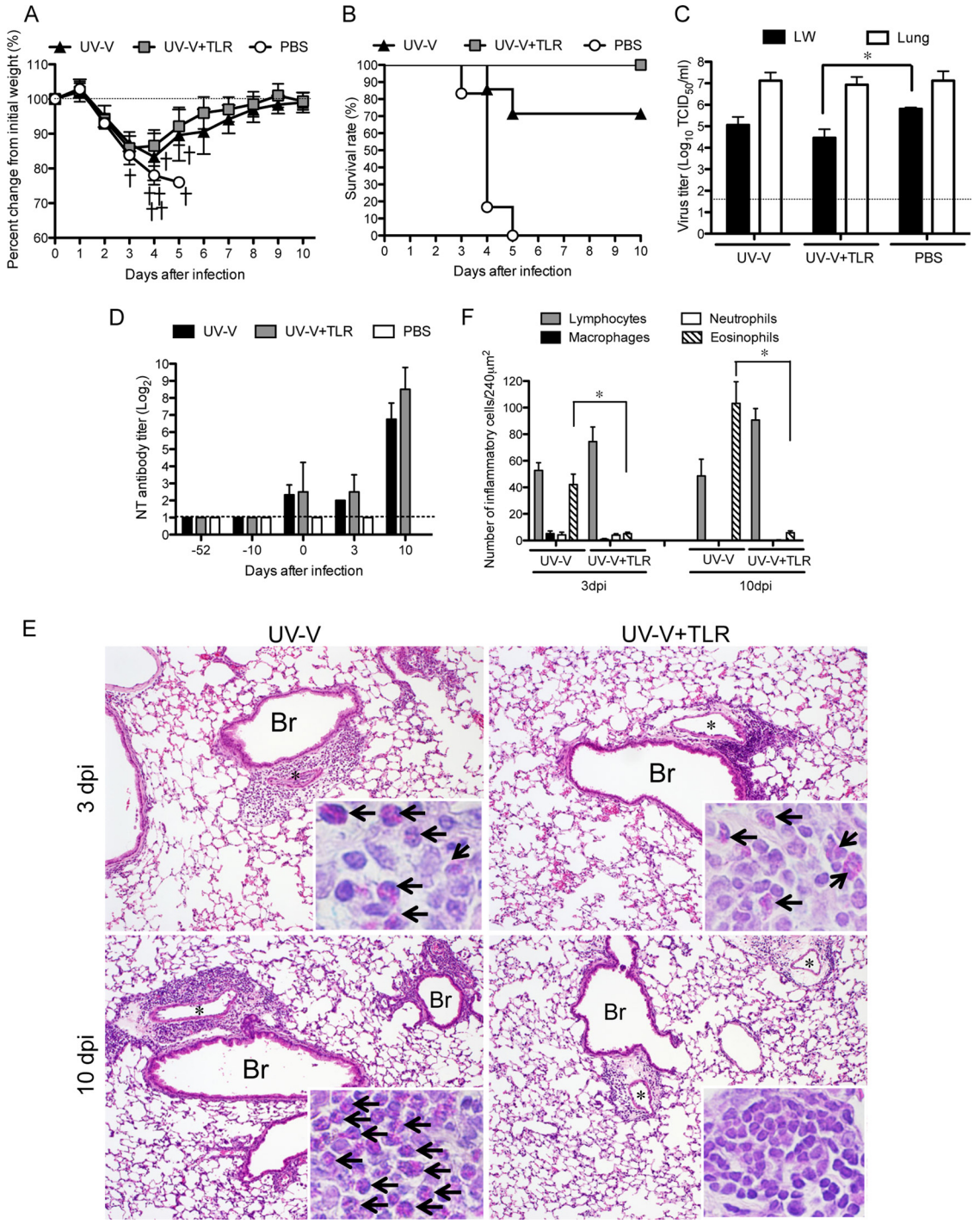

FIG 4 Immunization with UV-V and TLR agonists inhibits excessive eosinophilic infiltration after SARS-CoV challenge. Adult female BALB/c mice were vaccinated with UV-V, UV-V with TLR agonists (UV-V+TLR), or vehicle (PBS) and subsequently challenged with 1,000 $TCID_{50}$ of F-musX. Dead mice are marked with crosses. (A and B) Mice were weighed daily and monitored for morbidity ($n = 6$ to 7). (C) SARS-CoV titers in the lungs and lung wash fluids 3 days after intranasal challenge with SARS-CoV ($n = 4$). Significant differences ($P < 0.05$, one-way ANOVA) between groups are marked with an asterisk. The dashed line indicates the limit of detection ($10^{1.5}$ $TCID_{50}$/ml). Error bars indicate standard deviations. LW, lung wash fluid. (D) SARS-CoV-specific neutralizing serum antibody titers 52, 10, and 0 days before challenge ($n = 13$ to 14) and 3 and 10 days after challenge ($n = 6$ to 7, respectively) with SARS-CoV. Serum samples were 2-fold serially diluted beginning at 1:2. Error bars indicate standard deviations. (E) Representative images of lung sections from mice immunized with UV-V, UV-V+LPS, or UV-V+TLR on days 3 and 10 after challenge with F-musX. Hematoxylin-and-eosin (magnification, ×10) and C.E.M. kit (inset magnification, ×100) staining was used. Br, bronchi; *, blood vessel. (F) Numbers of lymphocytes, macrophages, neutrophils, and eosinophils in the lung sections ($n = 3$). Five 240-μm^2 regions in the extrabronchioles of lung per mouse were examined at magnification ×40. Asterisks indicate $P < 0.05$ by the Bonferroni test. Error bars indicate standard deviations.

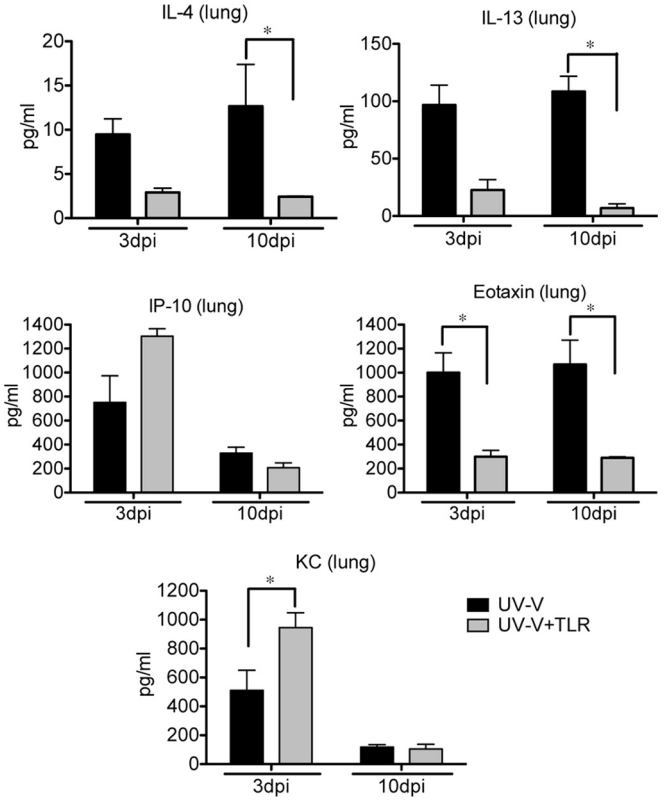

FIG 5 Cytokine and chemokine protein concentrations in lung homogenates of mice immunized with UV-V and challenged with SARS-CoV. The concentrations of cytokines and chemokines in lung homogenates were determined on days 3 and 10 after challenge ($n = 4$). Asterisks indicate significant differences ($P < 0.05$, one-way ANOVA). Error bars indicate standard deviations.

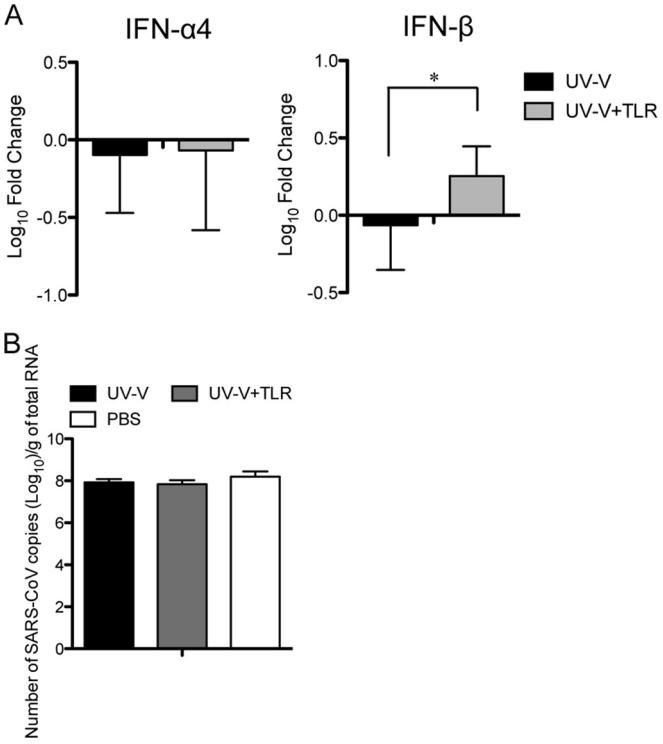

FIG 6 Type I IFN gene expression in lung homogenates of mice immunized with UV-V and challenged with SARS-CoV. Type I IFN mRNA expression profiles in UV-V- and UV-V+TLR-immunized mice (A) or amounts of viral RNA present during infection (B) are shown. RNA was taken from the lungs of UV-V- and UV-V+TLR-immunized mice 1 day after challenge. Type I IFN mRNAs and SARS-CoV genome (nsp11 region) were measured by quantitative real-time RT-PCR. Results are expressed as $\log_{10}$ fold change from results for mock-vaccinated, challenged mice. *, $P < 0.05$. Error bars indicate standard deviations.

Presence of eosinophil infiltration in the lungs after both short- and long-interval UV-V-immunization in response to virus challenge. A second vaccine experiment was performed to evaluate the long-term antiviral efficacy of UV-V+TLR. Fourteen mice per group were immunized with UV-V and UV-V+TLR and boosted 6 weeks later. Four weeks after boosting, the mice were intranasally challenged with F-musX. Both UV-V- and UV-V+TLR-immunized mice showed slight illness and mild loss of body weight but recovered by day 6 (Fig. 7A). Virus titers in the lungs and lung wash fluid on day 3 were below the limit of detection in both UV-V- and UV-V+TLR-immunized mice (Fig. 7B). One day before challenge, the serum titers of neutralizing antibodies were higher in both sets of immunized mice than in the previous experiment, shown in Fig. 4 (Fig. 7C). Microscopic analysis of the lung sections of UV-V-immunized mice 3 days after challenge showed eosinophil infiltration surrounding the bronchi and blood vessels (Fig. 7E), but the number was lower in these mice than in the mice challenged in the experiment shown in Fig. 4 (Fig. 7D). Eosinophil infiltration in the lung was lower on day 10 than on day 3 in UV-immunized mice. After long intervals, the UV-V- and UV-V+TLR-immunized mice seroconverted to produce sufficient neutralizing antibody against SARS-CoV infection. However, both short- and long-interval UV-V-immunization caused eosinophil infiltration in the lungs after challenge.

UV-V-immunized mice showed high expression of genes related to Th2 responses in the lungs after challenge. To better understand the biological pathways by which UV-V-induced pulmonary eosinophilia occurs, we examined global transcriptional changes in mouse lungs. Gene expression profiling was performed using total RNAs from the lungs of mice immunized with UV-V, UV-V+TLR, PBS (as a mock vaccination), or HKU39849 (mimicking live attenuated vaccine) 1 day after F-musX inoculation. A total of 242 genes were differentially regulated between UV-V- and UV-V+TLR-immunized mice. These data are plotted as a heat map, in which each entry represents a gene expression value (Fig. 8A). The data for PBS-injected and HKU39849-inoculated mice were also plotted on a heat map. UV-V- and UV-V+TLR-immunized mice elicited different patterns of gene expression associated with immune responses after SARS-CoV infection. Two trends were observed on the heat maps. Two hundred forty-two genes showed changes in expression level, with 107 genes upregulated and 135 genes downregulated in UV-V-immunized mice. Gene ontology analysis revealed that genes involved in the function, proliferation, differentiation, activation, and maturation of immune cells were expressed similarly, whereas genes associated with chemotaxis, eosinophil migration, eosinophilia, cell movement, and the polarization of Th2 cells were upregulated in UV-V-immunized mice (Table 2; see also Table S1 in the supplemental material) but downregulated in UV-V+TLR-immunized mice. Genes upregulated in UV-V+TLR-immunized mice included those associated with signaling of the proinflammatory cytokines

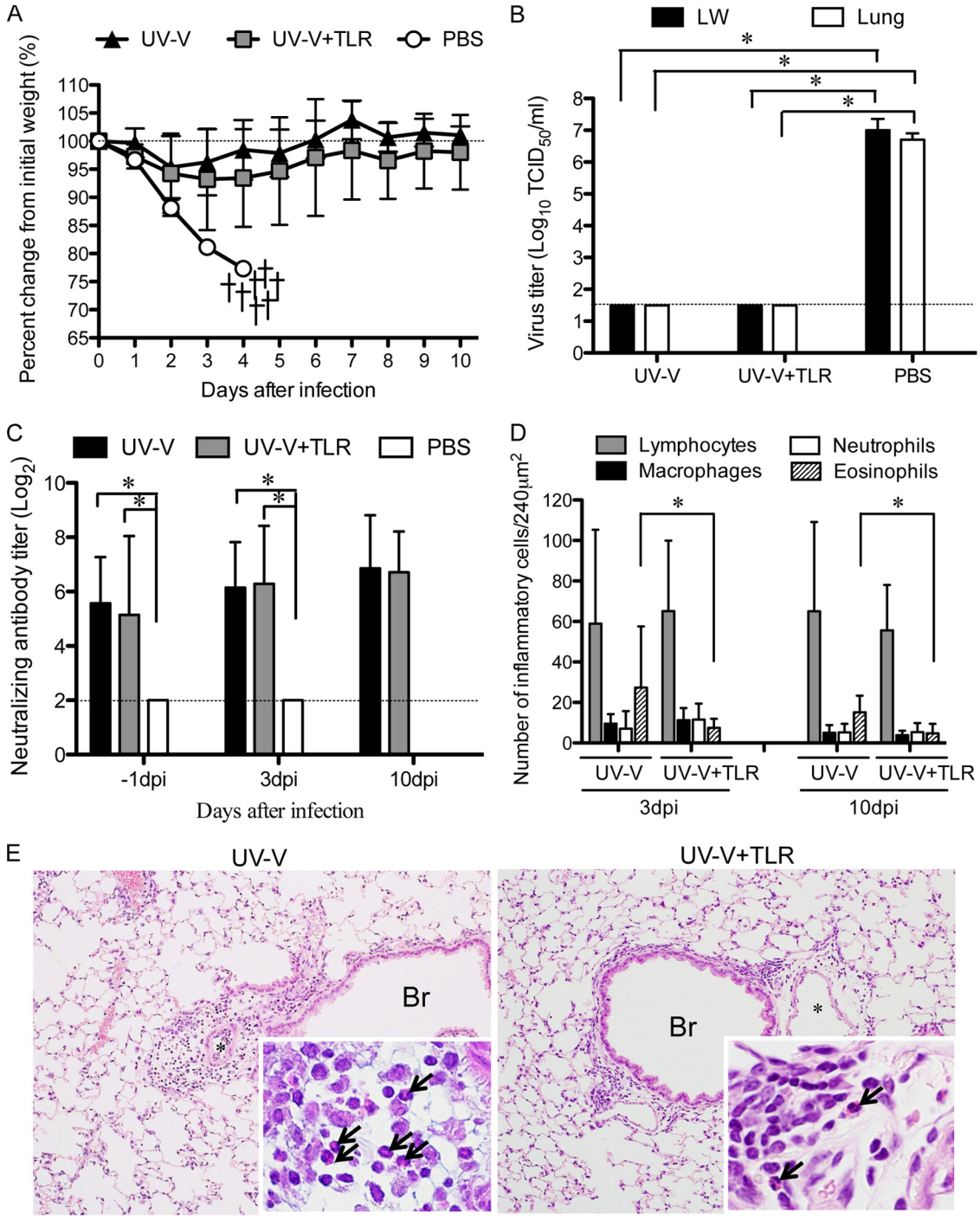

FIG 7 Immunization with UV-V or UV-V+TLR induces eosinophilic immune pathology in adult mice after long-term SARS-CoV challenge. Adult female BALB/c mice were vaccinated with UV-V or UV-V+TLR or mock vaccinated (PBS) and subsequently challenged with 1,000 $TCID_{50}$ of F-musX. (A) Body weight changes following the challenge inoculation ($n = 7$). Dead mice are marked with crosses. Error bars indicate the standard deviations. (B) Titers of virus in the lungs and lung wash fluids on day 3 postchallenge ($n = 4$). The dashed line indicates the limit of detection ($10^{1.5}$ $TCID_{50}$/ml). Error bars indicate standard deviations. Significant between-group differences ($P < 0.05$ by one-way ANOVA) are marked with an asterisk. LW, lung wash fluid. (C) Neutralizing serum antibody titers against SARS-CoV 1 day before challenge ($n = 14$) and 3 and 10 days after challenge ($n = 7$ each). Serum samples were 2-fold serially diluted beginning at 1:2. Error bars indicate standard deviations. Significant between-group differences ($P < 0.05$ by one-way ANOVA) are marked with an asterisk. (D) Numbers of lymphocytes, macrophages, neutrophils, and eosinophils in lung sections ($n = 3$). Five 240-μm^2 regions in the extrabronchioles in the lungs of each mouse were examined at magnification ×40. Asterisks indicate $P < 0.05$ by the Bonferroni test. Error bars indicate standard deviations. (E) Representative images of lung sections from UV-V-immunized (left panel) and UV-V+TLR-immunized (right panel) mice 3 days after challenge. Hematoxylin-and-eosin (magnification, ×10) and C.E.M. kit (inset; magnification, ×100) staining was used. Br, bronchi; ∗, blood vessel.

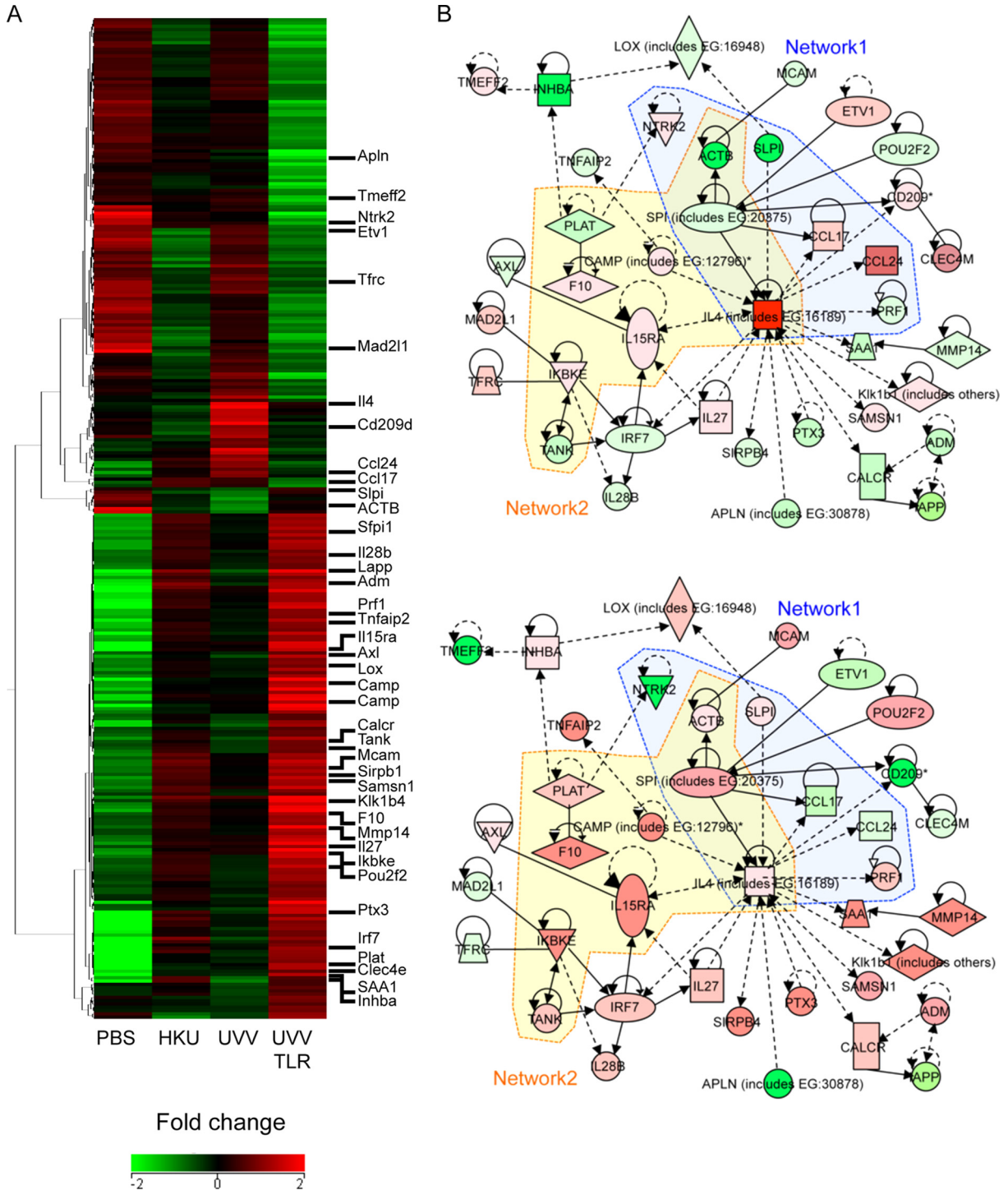

FIG 8 Global gene expression profiles of mice immunized with UV-V after SARS-CoV challenge. An ANOVA was performed to assess differences among all groups. All genes with a greater than 2.0-fold change ($P < 0.05$) in expression, relative to the median of the unchallenged groups, are depicted. Each row represents the lungs of a group of mice ($n = 3$, mock immunization with PBS (PBS); $n = 6$, inoculation with HKU39849 isolate (HKU), UV-V (UVV) or UV-V+TLR (UVVTLR)). The heat map shows the relative levels of expression of 305 probes (242 genes), confirmed statistically by direct comparisons between the UV-V and UV-V+TLR groups. The heat map was generated using the software program GeneSpring GX 12.1. (A) Uncentered Pearson correlation was used as the distance metric with average linkage for unsupervised hierarchical clustering. In the heat map, red represents high expression, black represents median expression, and green represents low expression. The color scale bar at the bottom indicates the relative level of expression. The sidebar on the right indicates genes that are closely related to each other. (B) A gene interaction network including 39 genes was constructed from 242 genes connected by IPA software. The solid and dotted lines indicate direct and indirect interactions, respectively. Genes shown in red were upregulated, and those shown in green were downregulated, compared with the PBS group. The central node is IL-4, a key cytokine in inflammation associated with eosinophils. Network 1 was composed of genes associated with eosinophilia. Network 2 was composed of genes associated with "inflammation of the lungs." The same network is shown for UV-V-immunized (upper panel) and UV-V+TLR-immunized (lower panel) mice.

TABLE 2 Top 5 biological function categories as determined by using IPA for early responses of mice immunized with UV-V and UV-V+TLR and subsequently challenged with SARS-CoV

Immunization	Function annotation	*P* value
UV-V	Eosinophil	7E−5 to 2E−2
	Function, proliferation, differentiation, activation, and maturation of immune cells	6E−5 to 3E−2
	Th2	6E−5 to 1E−2
	Cell movement of immune cells	5E−5 to 3E−2
	Responses to pathogen	3E−5 to 3E−2
UV-V+TLR	Cell movement of immune cells	8E−6 to 3E−3
	Function, proliferation, differentiation, activation, and maturation of immune cells	6E−5 to 3E−2
	Eosinophil	2E−2 to 1E−2
	Responses to pathogen	1E−4 to 2E−2
	Th2	NS[a]

[a] NS, not significant.

TNF-α1 and -2, both of which are regulated by TLRs, including TLR3 and TLR4 (Fig. 9). To assess the interconnection between genes during the host response to virus infection after UV-V immunization, a functional analysis approach was used to construct a graphic network of biologically related genes derived from IPA. This network was constructed by including the 242 genes differentially regulated between UV-V- and UV-V+TLR-immunized mice. Interestingly, this analysis yielded only one network, consisting of 39 of the 242 genes. The gene encoding IL-4 is at the center of this network (Fig. 8B). Network analysis revealed that differential gene regulation occurred independently, including the upregulation of the Th2-related chemokine thymus and activation-regulated chemokine (also called CCL17), eotaxin 2 (CCL24), and IL-4 in UV-V-immunized mice. The expression of the IL-4 and CCL24 genes was especially higher in the lungs of UV-V-immunized than in those of UV-V+TLR-immunized mice. These genes are associated with a network involving attraction, chemotaxis, accumulation, and stimulation of eosinophils. In addition, CCL17 and IL-4 are also associated with Th2 cell movement, homing, polarization, and arrest of proliferation. Most genes associated with "inflammation of the lungs" were unchanged or downregulated in UV-V-immunized mice compared with expression in UV-V+TLR-immunized mice, including actin, beta (ACTB), cathelicidin antimicrobial peptide (CAMP), coagulation factor X enzyme (F10), inhibitor of kappa light polypeptide gene enhancer in B cells, kinase epsilon (IKBKE), interleukin 15 receptor alpha (IL-15RA), IL-4, plasminogen activator, tissue (PLAT), spleen focus-forming virus proviral integration oncogene (SPI1), and TRAF family member-associated NF-κB activator (TANK) (Fig. 8B). Thus, both mRNA and protein assays for host immune responses revealed that the expression of genes related to Th2 responses, especially IL-4, had a key role in the excess eosinophilic immunopathology observed in the lungs of UV-V-immunized mice after subsequent SARS-CoV infection. Such unwanted side effects could be avoided by adding TLR antagonists as an adjuvant.

CD11b$^+$ cells in the lungs of UV-V-immunized mice show upregulation of genes associated with induction of eosinophils after challenge. In addition, gene expression analysis was analyzed in CD11b$^+$ cells, including macrophages, lymphocytes, and granulocytes, which express TLRs (26, 27). The purity of CD11b$^+$ cell populations was confirmed by flow cytometry after magnetic bead separation and was typically greater than 94% (Fig. 10A and D). Microscopic examination revealed that most of the sorted CD11b$^+$ cells were mononuclear small and large cells, but they also included polynuclear cells (Fig. 10B and E). A comparison of the gene expression profiles of CD11b$^+$ cells from UV-V- and UV-V+TLR-immunized mice showed that a total of 434 genes were differentially regulated. To dissect the temporal behavior of key players involved in TLR signaling in more detail, our data were analyzed using IPA. Upstream regulator analysis showed that certain genes were upstream regulators, including TLR3, TLR4, and poly(I·C) (see Table S2 in the supplemental material). To better understand the relationships of these genes, pathway networks were built. Although many networks could be constructed, we limited our investigation to the networks associated with the TLR3, -4, and -7 signaling pathways in order to understand the effect of treatment with TLR agonists on CD11b$^+$ cells. The network of differentially expressed genes related to TLR3, TLR4, and poly(I·C) is shown in Fig. 10C and F; a network for TLR7 could not be built from these data. The network involving TLR3, TLR4, and poly(I·C) consisted of 37 genes, many of which were associated with cellular movement, hematological system development and function, immune cell trafficking, inflammatory response, and infectious disease. There was no difference in gene expression in UV-V-immunized and UV-V+TLR-immunized mice following mock infection. The levels of expression of genes encoding solute carrier family 5, member 5 (SLC5A5), interferon regulatory factor 1 (IRF1), gamma interferon-induced GTPase (Igtp), immunity-related GTPase family M member 2 (Irgm2), interferon-inducible GTPase 1 (Iigp1), chemokine (C-X-C motif) ligand 9 (CXCL9), CD40, guanylate binding protein 4 (GBP4), and guanylate binding protein 2 (GBP2) were especially higher in CD11b$^+$ cells from UV-V+TLR-immunized than from UV-V-immunized mice. These genes were associated with cellular movement, recruitment of leukocytes, and maturation of antigen-presenting cells. In contrast, CD11b$^+$ cells from UV-V-immunized mice showed much more robust regulation of genes in this network than cells from UV-V+TLR-immunized mice. However, several of these genes, including those encoding CXCL2, plasminogen activator receptor (PLAUR), lactotransferrin (LTF), TNF-inducible gene 6 protein (TNFAIP6), CXCL9, and poly(I·C) RNA, have also been implicated in eosinophil migration and eosinophilia of the airways. IPA analysis revealed that these genes were also upregulated in CD11b$^+$ cells from the lungs of UV-V-immunized mice.

DISCUSSION

This study describes vaccine immunization, both with attenuated live and inactivated vaccines, and virus challenge using adult BALB/c mice and mouse-passaged SARS-CoV. This model is useful in the evaluation of efficacies and side effects of vaccine candidates. Several strategies have been considered for vaccination against SARS-CoV (reviewed in reference 28). Spike protein, but not envelope, membrane, or N proteins, protects vaccinated animals from SARS-CoV infection by inducing neutralizing antibodies (29–31) and strong cellular immunity. Antibodies detected in the sera of patients infected with SARS-CoV were directed against at least eight different proteins and bound to viral membranes (32). These findings indicate that multiple epitopes and proteins may be targets of protective antibodies. Although vaccination

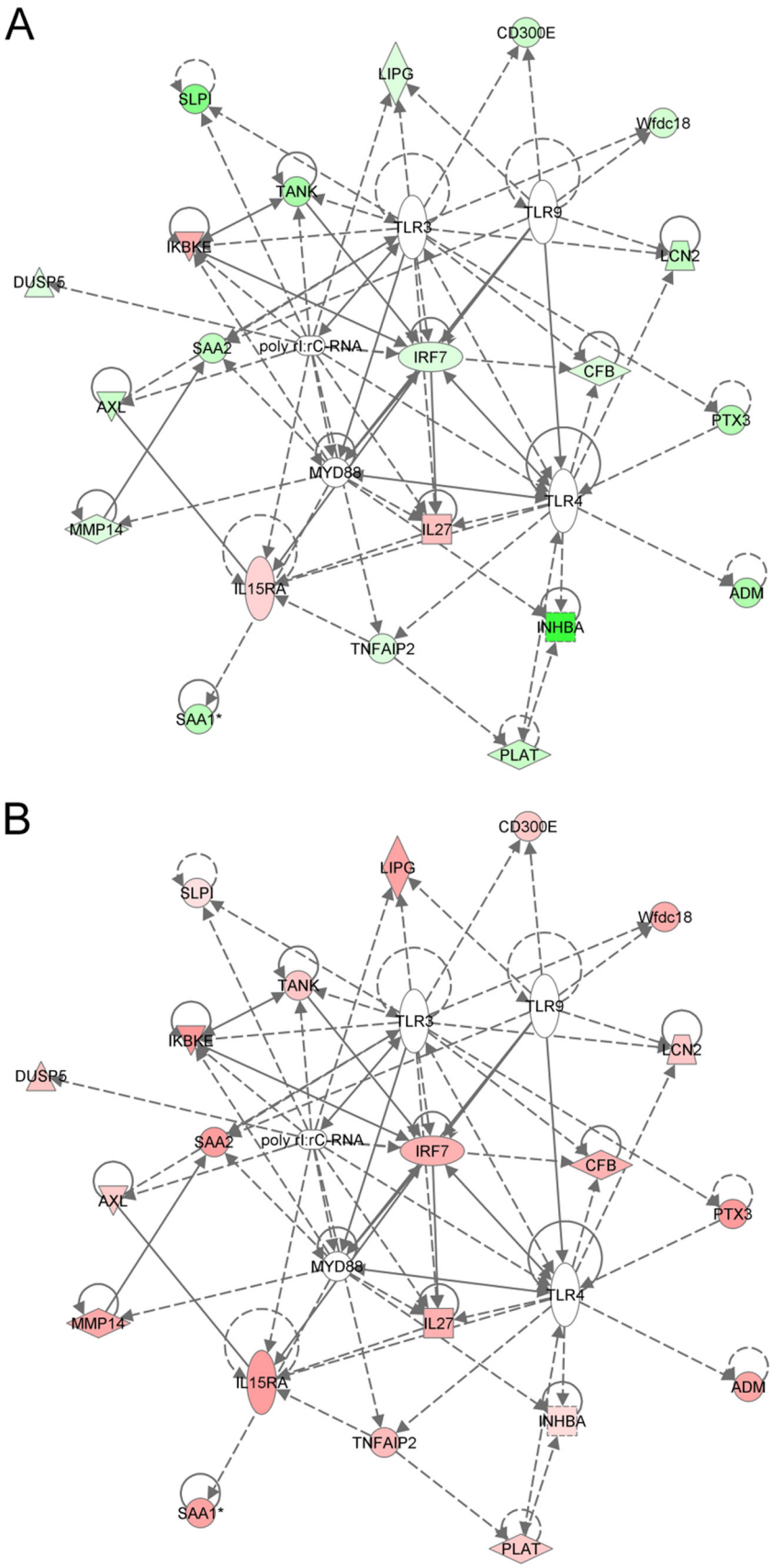

FIG 9 A network of genes in mice immunized with UV-V after SARS-CoV challenge. A direct comparison of gene expression profiles in the lungs of UV-V- and UV-V+TLR-immunized mice is shown. The diagrams show the TLR3 and TLR4 signaling pathways. Genes shown in red were upregulated, and those in green were downregulated, compared with expression for the PBS group. Several genes downstream of TLR3 and TLR4 signaling were upregulated in UV-V+TLR-immunized mice (B) compared with expression in UV-V-immunized mice (A). We overlaid gene expression data on the formed network using Ingenuity Pathway Analysis software.

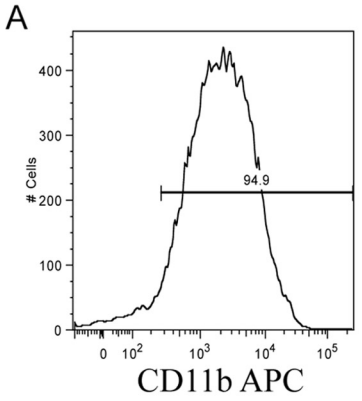
A
400
300
200
100
0
Cells
94.9
0
10^2
10^3
10^4
10^5
CD11b APC

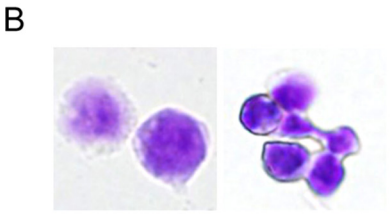
B

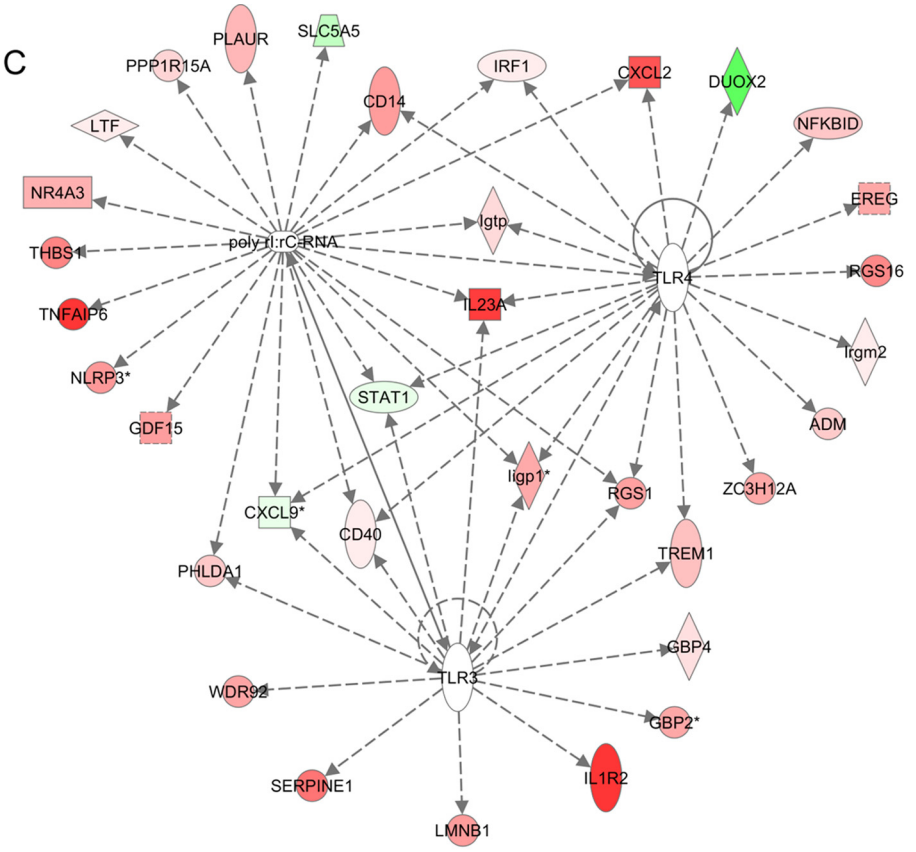
C
PLAUR
SLC5A5
PPP1R15A
IRF1
CXCL2
DUOX2
CD14
LTF
NFKBID
NR4A3
EREG
Igtp
THBS1
poly I:rC RNA
TLR4
RGS16
TNFAIP6
IL23A
Irgm2
NLRP3*
STAT1
ADM
GDF15
Iigp1*
RGS1
ZC3H12A
CXCL9*
CD40
TREM1
PHLDA1
GBP4
TLR3
WDR92
GBP2*
SERPINE1
IL1R2
LMNB1

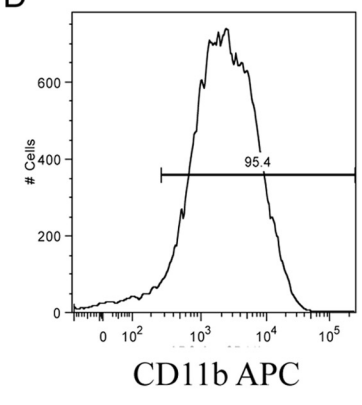
D
600
400
200
0
Cells
95.4
0
10^2
10^3
10^4
10^5
CD11b APC

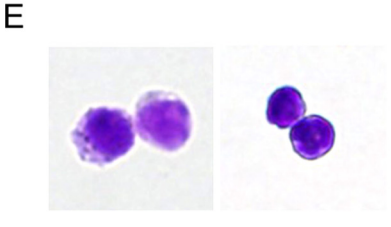
E

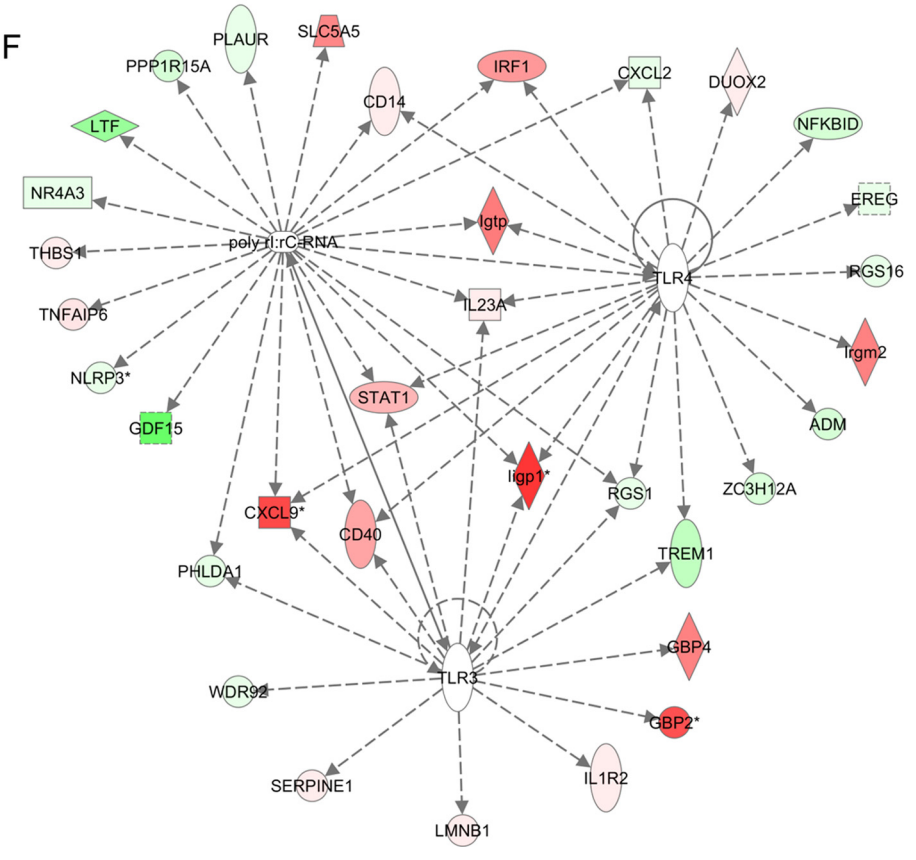
F
PLAUR
SLC5A5
PPP1R15A
IRF1
CXCL2
DUOX2
CD14
LTF
NFKBID
NR4A3
EREG
Igtp
THBS1
poly I:rC RNA
TLR4
RGS16
TNFAIP6
IL23A
Irgm2
NLRP3*
STAT1
ADM
GDF15
Iigp1*
RGS1
ZC3H12A
CXCL9*
CD40
TREM1
PHLDA1
GBP4
TLR3
WDR92
GBP2*
SERPINE1
IL1R2
LMNB1

with attenuated viruses is more efficacious than that with inactivated viruses due to their persistence in the host, attenuated viruses carry the risk of reversion of virulence or recombination repair (33). Due to safety concerns, it is often difficult to gain regulatory approval of attenuated vaccines without strong proof that the threat of disease is sufficient to warrant their use. This threshold has not yet been met for SARS, although some interesting attenuated mutants have been developed (34–36). In contrast, inactivated vaccines do not carry risks of mutating and reverting back to their virulent forms. UV-V virions have been successful due to large-scale production, the presentation of multiple epitopes, and the generation of high levels of humoral immunity in young BALB/c mice injected subcutaneously (37). However, SARS-CoV challenge has not been tested in more vulnerable animals.

In this study, we successfully evaluated the efficacy of UV-inactivated whole-virion immunization in a lethal adult mouse model of SARS-CoV infection. Adult BALB/c mice immunized with UV-V failed to inhibit viral infection and replication within the lungs on day 3. This was one cause of death after subsequent SARS-CoV infection and of enhanced lung immunopathology characterized by increased infiltration by eosinophils. These findings are consistent with studies of vaccine formulations incorporating SARS-CoV N protein and also SARS-CoV doubly inactivated with formalin and UV irradiation (11–14). An excessive host immune response against the N protein of SARS-CoV enhances eosinophilic infiltration into the lungs, resulting in a failure to inhibit viral replication and skewing the immune response toward Th2 responses (11–14). Similar lung pathology has also been observed in humans vaccinated with FI-RSV followed by RSV infection (38, 39), with the Th2-skewed cytokine profile also a hallmark of RSV vaccine-enhanced disease (40). The Th2-skewed cytokine profile is shown to be reduced only when the functions of IL-4 and IL-13, both Th2 cytokines, are blocked in FI-RSV-immunized mice (41, 42), indicating that both IL-4 and IL-13 promote the development of pulmonary eosinophilia upon RSV challenge of FI-RSV-immunized mice. High levels of Th2 cytokines, including IL-4 and IL-13, and the upregulation of genes associated with Th2 cell migration were observed in the lungs of UV-V-immunized mice, suggesting that the UV-V-specific immune response occurs in a manner similar to that of the FI-RSV vaccine. Furthermore, a few UV-V-immunized mice were unable to produce protective neutralizing antibodies and died on day 5 after challenge, showing severe inflammation, including high eosinophilia in the lungs. Interestingly, a UV-V+Alum-immunized mouse produced high titers of neutralizing antibodies in serum but died of eosinophilic pneumonia in this study. Vaccination with UV-inactivated virions of other viruses may carry a potential for dangerous clinical complications, similar to those observed for inactivated RSV vaccine. Pulmonary eosinophilia is a hallmark of an aberrant hypersensitivity response to FI-RSV (43). A recent study using eosinophil-deficient mice found that eosinophils did not contribute to RSV vaccine-enhanced pulmonary disease (44). In contrast, another study using mouse pneumonia virus, resulting in severe RSV, found that eosinophils did not promote virus clearance (45). The mechanism of vaccine-induced eosinophilia has not been determined, with no consensus as to whether eosinophils potentially contribute to protection or enhance lung immunopathology subsequent to respiratory infection.

Vaccine failure in RSV-enhanced respiratory disease was thought to be due to disruption of protective antigens by formalin. However, this lack of protection was due not to formalin-induced alterations but to low antibody avidity for protective epitopes resulting from poor TLR stimulation (18). To mimic live attenuated vaccine, mice were inoculated with HKU39849, which completely protected them from subsequent SARS-CoV infection. Moreover, these mice did not display enhanced eosinophilic infiltration in the lungs. In addition, all mock-vaccinated mice died but did not show evidence of eosinophilia. TLRs are critical to sensing invading microorganisms. Pathogen recognition by TLRs provokes the rapid activation of innate immunity, leading to effective adaptive immunity (23). Despite the protective effects of TLRs upon infection, faulty TLR signaling is increasingly implicated in the pathogenesis of allergic diseases (46, 47). We hypothesized that vaccination with UV-V was unable to generate effective immunity against SARS-CoV infection because of poor TLR stimulation, which may be enough when natural SARS-CoV infection occurs. In fact, immunizing mice with UV-V, together with the TLR agonists, poly(I·C) (a TLR3 agonist), LPS (a TLR4 agonist), and poly(U) (a TLR7 agonist), as an adjuvant, produced effective antibodies and inhibited excess eosinophilic immunopathology. The innate immunomodulatory activity in response to live and inactivated SARS-CoV is not well understood. However, mouse models of related CoV infection have suggested protective roles for TLR4 (48) and myeloid differentiation factor 88 (MyD88) (49), whereas TLR3 and TLR7 may be important for viral clearance through the production of type I IFN (50, 51).

Intranasal injection of the TLR agonist poly(I·C) into aged mice provided a high level of protection against SARS-CoV infection (51). Indeed, higher IFN-β gene expression on day 1 p.i. was seen in the lungs of UV-V+TLR-immunized mice than in those of UV-V-immunized mice. UV-V+TLR but not UV-V immunization primed the cells that expressed IFN-β after SARS-CoV infection. IFN-β was induced directly after Sendai virus infection in a murine model, leading to the expression of IFN-α genes (52). Although viral copy numbers in the lungs were similar in both groups 1 day after challenge, titers of virus differed significantly in the lung wash fluid of UV-V+TLR- and PBS-injected mice on day 3. Virus excretion into the lungs of UV-V+TLR-immunized mice on day 3 may be inhibited by IFN-β gene expression. The type I IFNs not only play an important role in the innate immune response but also enhance Th1-type responses (53). Higher IFN-β gene expression in UV-V+TLR-immunized mice may therefore contribute to the production of Th1 cytokines after viral infection.

FIG 10 Pathway analysis of the gene-to-gene networks of TLR3, TLR4, and poly(I·C) in mice immunized with UV-V after SARS-CoV challenge. Direct comparison of gene expression profiles in $CD11b^+$ cells isolated from the lungs of UV-V- and UV-V+TLR-immunized mice. (A and D) FACS analysis of enriched populations of $CD11b^+$ lung cells in UV-V-immunized (A) or UV-V+TLR-immunized (D) mice. Cells were prepared as described in Materials and Methods. (B and E) Conventional Giemsa staining of cytospins from populations of $CD11b^+$ lung cells in UV-V-immunized (B) or UV-V+TLR-immunized (E) mice (magnification, ×100). (C and F) Diagram showing the pathways of TLR3 and TLR4 signaling. Genes shown in red were upregulated, and those in green were downregulated. Several genes downstream of TLR3 and TLR4 signaling were upregulated in UV-V-immunized mice (C) compared with expression in UV-V+TLR-immunized mice (F). We overlaid gene expression data on the formed network by using Ingenuity Pathway Analysis software.

To assess the efficacy of vaccination of the mice, we demonstrated both short- and long-interval UV-V-immunization on virus challenge. The titer of neutralizing antibodies was higher after a longer period of time, and these antibodies were sufficiently protective against SARS-CoV infection. However, eosinophil infiltration in the lungs occurred in the UV-V-immunized mice.

Mice immunized with inactivated RSV plus TLR agonists produced mature antibodies following TLR stimulation, preventing enhanced respiratory disease (18). These findings suggest that TLR stimulation during immunization with UV-V plays a key role in reducing eosinophil infiltration into the lungs, with strong TLR stimulation by TLR agonists shifting the host immune response in the lungs from Th2 to Th1. In line with this, our microarray analysis showed that several genes downstream of TLR3 and TLR4 signaling were markedly upregulated in UV-V+TLR-immunized mice compared with expression in UV-V-immunized mice on day 1 after subsequent SARS-CoV infection. Furthermore, IPA analysis of $CD11b^+$ cells isolated from the lungs of UV-V+TLR-immunized mice showed upregulation of genes associated with cellular movement and maturation of antigen-presenting cells in the TLR3 and TLR4 signaling pathways. This finding indicated that UV-V+TLR but not UV-V immunization may prime effective innate immune responses against SARS-CoV infection in mice due to the intensity of TLR stimulation.

To our knowledge, this is the first study to show that vaccination with UV-inactivated whole virions plus TLR agonists provides protection against SARS-CoV infection without strong Th2 skewing; TLR stimulation reduced the high level of eosinophilic infiltration that occurred in the lungs of mice immunized with UV-V. TLR agonists are approved for human use (54), and several are currently in preclinical development for use as vaccine adjuvants (55). Further studies regarding the association of TLR stimulation with protective immunity to SARS-CoV infection, the indication that eosinophils contribute to the negative sequelae of disease, and the mechanisms of eosinophil recruitment to lung tissue are required.

ACKNOWLEDGMENTS

This work was supported by a Grant-in Aid for Young Scientists (B), no. 22790444, from the Japan Society for the Promotion of Science and Grants-in Aid for research on emerging and reemerging infectious diseases, H23-Shinko-Ippan-007 and H25-Shinko-Wakate-004, from the Ministry of Health, Labor, and Welfare, Japan.

We thank our colleagues at the institute, especially Ayako Harashima and Mihoko Fujino, for their technical assistance and Shin-ichi Tamura for valuable discussions.

REFERENCES

1. **Drosten C, Gunther S, Preiser W, van der Werf S, Brodt HR, Becker S, Rabenau H, Panning M, Kolesnikova L, Fouchier RA, Berger A, Burguiere AM, Cinatl J, Eickmann M, Escriou N, Grywna K, Kramme S, Manuguerra JC, Muller S, Rickerts V, Sturmer M, Vieth S, Klenk HD, Osterhaus AD, Schmitz H, Doerr HW.** 2003. Identification of a novel coronavirus in patients with severe acute respiratory syndrome. N. Engl. J. Med. **348:**1967–1976. http://dx.doi.org/10.1056/NEJMoa030747.
2. **Ksiazek TG, Erdman D, Goldsmith CS, Zaki SR, Peret T, Emery S, Tong S, Urbani C, Comer JA, Lim W, Rollin PE, Dowell SF, Ling AE, Humphrey CD, Shieh WJ, Guarner J, Paddock CD, Rota P, Fields B, DeRisi J, Yang JY, Cox N, Hughes JM, LeDuc JW, Bellini WJ, Anderson LJ.** 2003. A novel coronavirus associated with severe acute respiratory syndrome. N. Engl. J. Med. **348:**1953–1966. http://dx.doi.org/10.1056/NEJMoa030781.
3. **Peiris JSM, Lai ST, Poon LLM, Guan Y, Yam LYC, Lim W, Nicholls J, Yee WKS, Yan WW, Cheung MT, Cheng VCC, Chan KH, Tsang DNC, Yung RWH, Ng TK, Yuen KY.** 2003. Coronavirus as a possible cause of severe acute respiratory syndrome. Lancet **361:**1319–1325. http://dx.doi.org/10.1016/S0140-6736(03)13077-2.
4. **Rota PA, Oberste MS, Monroe SS, Nix WA, Campagnoli R, Icenogle JP, Penaranda S, Bankamp B, Maher K, Chen MH, Tong S, Tamin A, Lowe L, Frace M, DeRisi JL, Chen Q, Wang D, Erdman DD, Peret TC, Burns C, Ksiazek TG, Rollin PE, Sanchez A, Liffick S, Holloway B, Limor J, McCaustland K, Olsen-Rasmussen M, Fouchier R, Gunther S, Osterhaus AD, Drosten C, Pallansch MA, Anderson LJ, Bellini WJ.** 2003. Characterization of a novel coronavirus associated with severe acute respiratory syndrome. Science **300:**1394–1399. http://dx.doi.org/10.1126/science.1085952.
5. **He Y, Zhou Y, Siddiqui P, Jiang S.** 2004. Inactivated SARS-CoV vaccine elicits high titers of spike protein-specific antibodies that block receptor binding and virus entry. Biochem. Biophys. Res. Commun. **325:**445–452. http://dx.doi.org/10.1016/j.bbrc.2004.10.052.
6. **Takasuka N, Fujii H, Takahashi Y, Kasai M, Morikawa S, Itamura S, Ishii K, Sakaguchi M, Ohnishi K, Ohshima M, Hashimoto S, Odagiri T, Tashiro M, Yoshikura H, Takemori T, Tsunetsugu-Yokota Y.** 2004. A subcutaneously injected UV-inactivated SARS coronavirus vaccine elicits systemic humoral immunity in mice. Int. Immunol. **16:**1423–1430. http://dx.doi.org/10.1093/intimm/dxh143.
7. **Tang L, Zhu Q, Qin E, Yu M, Ding Z, Shi H, Cheng X, Wang C, Chang G, Zhu Q, Fang F, Chang H, Li S, Zhang X, Chen X, Yu J, Wang J, Chen Z.** 2004. Inactivated SARS-CoV vaccine prepared from whole virus induces a high level of neutralizing antibodies in BALB/c mice. DNA Cell Biol. **23:**391–394. http://dx.doi.org/10.1089/104454904323145272.
8. **Xiong S, Wang YF, Zhang MY, Liu XJ, Zhang CH, Liu SS, Qian CW, Li JX, Lu JH, Wan ZY, Zheng HY, Yan XG, Meng MJ, Fan JL.** 2004. Immunogenicity of SARS inactivated vaccine in BALB/c mice. Immunol. Lett. **95:**139–143. http://dx.doi.org/10.1016/j.imlet.2004.06.014.
9. **Qu D, Zheng B, Yao X, Guan Y, Yuan ZH, Zhong NS, Lu LW, Xie JP, Wen YM.** 2005. Intranasal immunization with inactivated SARS-CoV (SARS-associated coronavirus) induced local and serum antibodies in mice. Vaccine **23:**924–931. http://dx.doi.org/10.1016/j.vaccine.2004.07.031.
10. **Zhang CH, Lu JH, Wang YF, Zheng HY, Xiong S, Zhang MY, Liu XJ, Li JX, Wan ZY, Yan XG, Qi SY, Cui Z, Zhang B.** 2005. Immune responses in Balb/c mice induced by a candidate SARS-CoV inactivated vaccine prepared from F69 strain. Vaccine **23:**3196–3201. http://dx.doi.org/10.1016/j.vaccine.2004.11.073.
11. **Deming D, Sheahan T, Heise M, Yount B, Davis N, Sims A, Suthar M, Harkema J, Whitmore A, Pickles R, West A, Donaldson E, Curtis K, Johnston R, Baric R.** 2006. Vaccine efficacy in senescent mice challenged with recombinant SARS-CoV bearing epidemic and zoonotic spike variants. PLoS Med. **3:**e525. http://dx.doi.org/10.1371/journal.pmed.0030525.
12. **Yasui F, Kai C, Kitabatake M, Inoue S, Yoneda M, Yokochi S, Kase R, Sekiguchi S, Morita K, Hishima T, Suzuki H, Karamatsu K, Yasutomi Y, Shida H, Kidokoro M, Mizuno K, Matsushima K, Kohara M.** 2008. Prior immunization with severe acute respiratory syndrome (SARS)-associated coronavirus (SARS-CoV) nucleocapsid protein causes severe pneumonia in mice infected with SARS-CoV. J. Immunol. **181:**6337–6348. http://dx.doi.org/10.4049/jimmunol.181.9.6337.
13. **Bolles M, Deming D, Long K, Agnihothram S, Whitmore A, Ferris M, Funkhouser W, Gralinski L, Totura A, Heise M, Baric RS.** 2011. A double-inactivated severe acute respiratory syndrome coronavirus vaccine provides incomplete protection in mice and induces increased eosinophilic proinflammatory pulmonary response upon challenge. J. Virol. **85:**12201–12215. http://dx.doi.org/10.1128/JVI.06048-11.
14. **Tseng CT, Sbrana E, Iwata-Yoshikawa N, Newman PC, Garron T, Atmar RL, Peters CJ, Couch RB.** 2012. Immunization with SARS coronavirus vaccines leads to pulmonary immunopathology on challenge with the SARS virus. PLoS One **7:**e35421. http://dx.doi.org/10.1371/journal.pone.0035421.
15. **Neuman BW, Adair BD, Yoshioka C, Quispe JD, Orca G, Kuhn P, Milligan RA, Yeager M, Buchmeier MJ.** 2006. Supramolecular architecture of severe acute respiratory syndrome coronavirus revealed by electron cryomicroscopy. J. Virol. **80:**7918–7928. http://dx.doi.org/10.1128/JVI.00645-06.
16. **Kim HW, Canchola JG, Brandt CD, Pyles G, Chanock RM, Jensen K, Parrott RH.** 1969. Respiratory syncytial virus disease in infants despite prior administration of antigenic inactivated vaccine. Am. J. Epidemiol. **89:**422–434.

17. **Olson MR, Varga SM.** 2008. Pulmonary immunity and immunopathology: lessons from respiratory syncytial virus. Expert Rev. Vaccines **7:**1239–1255. http://dx.doi.org/10.1586/14760584.7.8.1239.
18. **Delgado MF, Coviello S, Monsalvo AC, Melendi GA, Hernandez JZ, Batalle JP, Diaz L, Trento A, Chang HY, Mitzner W, Ravetch J, Melero JA, Irusta PM, Polack FP.** 2009. Lack of antibody affinity maturation due to poor Toll-like receptor stimulation leads to enhanced respiratory syncytial virus disease. Nat. Med. **15:**34–41. http://dx.doi.org/10.1038/nm.1894.
19. **Nagata N, Iwata N, Hasegawa H, Fukushi S, Harashima A, Sato Y, Saijo M, Taguchi F, Morikawa S, Sata T.** 2008. Mouse-passaged severe acute respiratory syndrome-associated coronavirus leads to lethal pulmonary edema and diffuse alveolar damage in adult but not young mice. Am. J. Pathol. **172:**1625–1637. http://dx.doi.org/10.2353/ajpath.2008.071060.
20. **Nagata N, Iwata N, Hasegawa H, Sato Y, Morikawa S, Saijo M, Itamura S, Saito T, Ami Y, Odagiri T, Tashiro M, Sata T.** 2007. Pathology and virus dispersion in cynomolgus monkeys experimentally infected with severe acute respiratory syndrome coronavirus via different inoculation routes. Int. J. Exp. Pathol. **88:**403–414. http://dx.doi.org/10.1111/j.1365-2613.2007.00567.x.
21. **Zhang X, Goncalves R, Mosser DM.** 2008. The isolation and characterization of murine macrophages. Curr. Protoc. Immunol. **83:**14.1–14.1.14. http://dx.doi.org/10.1002/0471142735.im1401s83.
22. **Sugiura N, Uda A, Inoue S, Kojima D, Hamamoto N, Kaku Y, Okutani A, Noguchi A, Park CH, Yamada A.** 2011. Gene expression analysis of host innate immune responses in the central nervous system following lethal CVS-11 infection in mice. Jpn. J. Infect. Dis. **64:**463–472.
23. **Kaisho T, Akira S.** 2002. Toll-like receptors as adjuvant receptors. Biochim. Biophys. Acta **1589:**1–13. http://dx.doi.org/10.1016/S0167-4889(01)00182-3.
24. **Pashine A, Valiante NM, Ulmer JB.** 2005. Targeting the innate immune response with improved vaccine adjuvants. Nat. Med. **11:**S63–S68. http://dx.doi.org/10.1038/nm1210.
25. **O'Neill LA, Bowie AG.** 2007. The family of five: TIR-domain-containing adaptors in Toll-like receptor signalling. Nat. Rev. Immunol. **7:**353–364. http://dx.doi.org/10.1038/nri2079.
26. **O'Mahony DS, Pham U, Iyer R, Hawn TR, Liles WC.** 2008. Differential constitutive and cytokine-modulated expression of human Toll-like receptors in primary neutrophils, monocytes, and macrophages. Int. J. Med. Sci. **5:**1–8. http://dx.doi.org/10.7150/ijms.5.1.
27. **Applequist SE, Wallin RP, Ljunggren HG.** 2002. Variable expression of Toll-like receptor in murine innate and adaptive immune cell lines. Int. Immunol. **14:**1065–1074. http://dx.doi.org/10.1093/intimm/dxf069.
28. **Roper RL, Rehm KE.** 2009. SARS vaccines: where are we? Expert Rev. Vaccines **8:**887–898. http://dx.doi.org/10.1586/erv.09.43.
29. **Buchholz UJ, Bukreyev A, Yang L, Lamirande EW, Murphy BR, Subbarao K, Collins PL.** 2004. Contributions of the structural proteins of severe acute respiratory syndrome coronavirus to protective immunity. Proc. Natl. Acad. Sci. U. S. A. **101:**9804–9809. http://dx.doi.org/10.1073/pnas.0403492101.
30. **Bukreyev A, Lamirande EW, Buchholz UJ, Vogel LN, Elkins WR, St Claire M, Murphy BR, Subbarao K, Collins PL.** 2004. Mucosal immunisation of African green monkeys (Cercopithecus aethiops) with an attenuated parainfluenza virus expressing the SARS coronavirus spike protein for the prevention of SARS. Lancet **363:**2122–2127. http://dx.doi.org/10.1016/S0140-6736(04)16501-X.
31. **Ishii K, Hasegawa H, Nagata N, Mizutani T, Morikawa S, Suzuki T, Taguchi F, Tashiro M, Takemori T, Miyamura T, Tsunetsugu-Yokota Y.** 2006. Induction of protective immunity against severe acute respiratory syndrome coronavirus (SARS-CoV) infection using highly attenuated recombinant vaccinia virus DIs. Virology **351:**368–380. http://dx.doi.org/10.1016/j.virol.2006.03.020.
32. **Guo JP, Petric M, Campbell W, McGeer PL.** 2004. SARS corona virus peptides recognized by antibodies in the sera of convalescent cases. Virology **324:**251–256. http://dx.doi.org/10.1016/j.virol.2004.04.017.
33. **Hanley KA.** 2011. The double-edged sword: how evolution can make or break a live-attenuated virus vaccine. Evolution **4:**635–643. http://dx.doi.org/10.1007/s12052-011-0365-y.
34. **DeDiego ML, Alvarez E, Almazan F, Rejas MT, Lamirande E, Roberts A, Shieh WJ, Zaki SR, Subbarao K, Enjuanes L.** 2007. A severe acute respiratory syndrome coronavirus that lacks the E gene is attenuated in vitro and in vivo. J. Virol. **81:**1701–1713. http://dx.doi.org/10.1128/JVI.01467-06.
35. **Dediego ML, Pewe L, Alvarez E, Rejas MT, Perlman S, Enjuanes L.** 2008. Pathogenicity of severe acute respiratory coronavirus deletion mutants in hACE-2 transgenic mice. Virology **376:**379–389. http://dx.doi.org/10.1016/j.virol.2008.03.005.
36. **Lamirande EW, DeDiego ML, Roberts A, Jackson JP, Alvarez E, Sheahan T, Shieh WJ, Zaki SR, Baric R, Enjuanes L, Subbarao K.** 2008. A live attenuated severe acute respiratory syndrome coronavirus is immunogenic and efficacious in golden Syrian hamsters. J. Virol. **82:**7721–7724. http://dx.doi.org/10.1128/JVI.00304-08.
37. **Tsunetsugu-Yokota Y.** 2008. Large-scale preparation of UV-inactivated SARS coronavirus virions for vaccine antigen. Methods Mol. Biol. **454:**119–126. http://dx.doi.org/10.1007/978-1-59745-181-9_11.
38. **Hancock GE, Speelman DJ, Heers K, Bortell E, Smith J, Cosco C.** 1996. Generation of atypical pulmonary inflammatory responses in BALB/c mice after immunization with the native attachment (G) glycoprotein of respiratory syncytial virus. J. Virol. **70:**7783–7791.
39. **De Swart RL, Kuiken T, Timmerman HH, van Amerongen G, Van Den Hoogen BG, Vos HW, Neijens HJ, Andeweg AC, Osterhaus AD.** 2002. Immunization of macaques with formalin-inactivated respiratory syncytial virus (RSV) induces interleukin-13-associated hypersensitivity to subsequent RSV infection. J. Virol. **76:**11561–11569. http://dx.doi.org/10.1128/JVI.76.22.11561-11569.2002.
40. **Johnson TR, Varga SM, Braciale TJ, Graham BS.** 2004. Vbeta14(+) T cells mediate the vaccine-enhanced disease induced by immunization with respiratory syncytial virus (RSV) G glycoprotein but not with formalin-inactivated RSV. J. Virol. **78:**8753–8760. http://dx.doi.org/10.1128/JVI.78.16.8753-8760.2004.
41. **Johnson TR, Graham BS.** 1999. Secreted respiratory syncytial virus G glycoprotein induces interleukin-5 (IL-5), IL-13, and eosinophilia by an IL-4-independent mechanism. J. Virol. **73:**8485–8495.
42. **Johnson TR, Parker RA, Johnson JE, Graham BS.** 2003. IL-13 is sufficient for respiratory syncytial virus G glycoprotein-induced eosinophilia after respiratory syncytial virus challenge. J. Immunol. **170:**2037–2045. http://dx.doi.org/10.4049/jimmunol.170.4.2037.
43. **Rosenberg HF, Dyer KD, Domachowske JB.** 2009. Respiratory viruses and eosinophils: exploring the connections. Antiviral Res. **83:**1–9. http://dx.doi.org/10.1016/j.antiviral.2009.04.005.
44. **Castilow EM, Legge KL, Varga SM.** 2008. Cutting edge: eosinophils do not contribute to respiratory syncytial virus vaccine-enhanced disease. J. Immunol. **181:**6692–6696. http://dx.doi.org/10.4049/jimmunol.181.10.6692.
45. **Percopo CM, Qiu Z, Phipps S, Foster PS, Domachowske JB, Rosenberg HF.** 2009. Pulmonary eosinophils and their role in immunopathologic responses to formalin-inactivated pneumonia virus of mice. J. Immunol. **183:**604–612. http://dx.doi.org/10.4049/jimmunol.0802270.
46. **Horner AA, Raz E.** 2003. Do microbes influence the pathogenesis of allergic diseases? Building the case for Toll-like receptor ligands. Curr. Opin. Immunol. **15:**614–619. http://dx.doi.org/10.1016/j.coi.2003.09.021.
47. **Vercelli D.** 2006. Mechanisms of the hygiene hypothesis—molecular and otherwise. Curr. Opin. Immunol. **18:**733–737. http://dx.doi.org/10.1016/j.coi.2006.09.002.
48. **Khanolkar A, Hartwig SM, Haag BA, Meyerholz DK, Harty JT, Varga SM.** 2009. Toll-like receptor 4 deficiency increases disease and mortality after mouse hepatitis virus type 1 infection of susceptible C3H mice. J. Virol. **83:**8946–8956. http://dx.doi.org/10.1128/JVI.01857-08.
49. **Sheahan T, Morrison TE, Funkhouser W, Uematsu S, Akira S, Baric RS, Heise MT.** 2008. MyD88 is required for protection from lethal infection with a mouse-adapted SARS-CoV. PLoS Pathog. **4:**e1000240. http://dx.doi.org/10.1371/journal.ppat.1000240.
50. **Cervantes-Barragan L, Zust R, Weber F, Spiegel M, Lang KS, Akira S, Thiel V, Ludewig B.** 2007. Control of coronavirus infection through plasmacytoid dendritic-cell-derived type I interferon. Blood **109:**1131–1137. http://dx.doi.org/10.1182/blood-2006-05-023770.
51. **Zhao J, Wohlford-Lenane C, Zhao J, Fleming E, Lane TE, McCray PB, Jr, Perlman S.** 2012. Intranasal treatment with poly(I·C) protects aged mice from lethal respiratory virus infections. J. Virol. **86:**11416–11424. http://dx.doi.org/10.1128/JVI.01410-12.
52. **Erlandsson L, Blumenthal R, Eloranta ML, Engel H, Alm G, Weiss S, Leanderson T.** 1998. Interferon-beta is required for interferon-alpha production in mouse fibroblasts. Curr. Biol. **8:**223–226. http://dx.doi.org/10.1016/S0960-9822(98)70086-7.
53. **Biron CA.** 1998. Role of early cytokines, including alpha and beta interferons (IFN-alpha/beta), in innate and adaptive immune responses to

viral infections. Semin. Immunol. **10:**383–390. http://dx.doi.org/10.1006/smim.1998.0138.
54. **Kanzler H, Barrat FJ, Hessel EM, Coffman RL.** 2007. Therapeutic targeting of innate immunity with Toll-like receptor agonists and antagonists. Nat. Med. **13:**552–559. http://dx.doi.org/10.1038/nm1589.
55. **Horscroft NJ, Pryde DC, Bright H.** 2012. Antiviral applications of Toll-like receptor agonists. J. Antimicrob. Chemother. **67:**789–801. http://dx.doi.org/10.1093/jac/dkr588.
56. **Keyaerts E, Vijgen L, Maes P, Duson G, Neyts J, Van Ranst M.** 2006. Viral load quantitation of SARS-coronavirus RNA using a one-step real-time RT-PCR. Int. J. Infect. Dis. **10:**32–37. http://dx.doi.org/10.1016/j.ijid.2005.02.003.